JOURNAL OF GEOPHYSICAL RESEARCH, VOL. 105, NO. B12, PAGES 27,895–27,915, DECEMBER 10, 2000

Deformation properties of subfreezing glacier ice: Role of crystal size, chemical impurities, and rock particles inferred from in situ measurements

K. M. Cuffey,[1] H. Conway,[2] A. Gades,[2] B. Hallet,[3] C. F. Raymond,[2] and S. Whitlow[4]

Abstract. To improve understanding of the deformation properties of subfreezing polycrystalline glacier ice and, in particular the role of crystal size, chemical impurities, and rock particle impurities, we analyze in situ strain rates of the basal layers of Meserve Glacier, Antarctica. Strain rates were monitored on the walls of a subglacial tunnel (where down flow shear stress is relatively uniform) and ice properties were measured (texture, fabric, and impurity content). We propose a simple empirical model describing strain rate variations due to variations in crystal size and impurity content, and we use all relevant Meserve data to constrain model parameters. We conclude that there is a direct dependence of strain rate on crystal size, which reflects an important role for a grain-size-sensitive deformation mechanism such as grain boundary sliding or diffusion. Chemical impurities are found to enhance the grain-size-sensitive deformation and are found to be an important control on strain rate variations in the very impure ices of Meserve Glacier. However, the per molar sensitivity of strain rate to chemical impurity content is shown to be very low, such that in the ice age ices of the Greenland ice sheet there is probably an immeasurable contribution of chemical impurities to strain rate enhancement, though we cannot exclude chemical enhancements as high as 1.3 there. Our analyses detect no direct rheologic effect of rock particles in the Meserve ices, which suggests that rock content is not directly responsible for the low viscosity of dirty basal layers.

1. Introduction

An appropriate rheologic relation for polycrystalline ice is a keystone in our understanding of Earth's ice sheets and glaciers. The empirical rheologic relation most used by glaciologists is the generalized Glen's law [*Glen*, 1955; *Nye*, 1957; *Paterson*, 1994], which describes strain rate as a nonlinear function of stress and temperature. Glen's law (hereinafter GL) is usually interpreted to be a manifestation of dislocation motion, a combination of easy glide on basal planes and dislocation climb normal to basal planes [*Duval et al.*, 1983; *Alley*, 1992; *Castelnau et al.*, 1996], the latter being rate limiting. A rheology dominantly reflecting these mechanisms is independent of crystal size. Incompatible deformations in polycrystals may be accommodated by diffusional creep, which is crystal-size-dependent, but this mechanism has not been suggested to control ice deformation.

Several decades ago, *Barnes et al.* [1971] recognized that the increase of apparent activation energy in GL at temperatures approaching the melting point (greater than about -10°C) most likely reflects an increasing role for a deformation mechanism, such as grain boundary sliding, and accommodation by transport along grain boundaries, possibly in liquid films. Recently, *Goldsby and Kohlstedt* [1997] and *Peltier* [1998] have argued that at stresses typical of terrestrial ice, GL reflects important contributions from grain boundary sliding at all Earth temperatures, even at grain sizes of order 10^{-3} m. An important consequence of grain boundary sliding is that polycrystalline ice rheology will depend importantly on grain size [*Barnes et al.*, 1971; *Goldsby and Kohlstedt*, 1997] (a grain is a single crystal for most applications in glaciology). No grain size dependence is permitted in the usual implementation of Glen's law.

Recent experiments of *De La Chapelle et al.* [1999] suggest that mass transport along grain boundaries reduces stress concentrations in polycrystals and there-

[1]Department of Geography and Department of Earth and Planetary Science, University of California, Berkeley.
[2]Geophysics Program, University of Washington, Seattle.
[3]Quaternary Research Center, University of Washington, Seattle.
[4]Climate Change Research Center, University of New Hampshire, Durham.

Copyright 2000 by the American Geophysical Union.

Paper number 2000JB900271.
0148-0227/00/2000JB900271$09.00

fore reduces bulk viscosity by increasing the ratio of easy glide to hard glide in dislocation creep. It is not clear whether this implies a grain size dependence of the viscosity or not. The *De La Chapelle et al.* [1999] experiments were conducted on ices with water contents very much higher than are typical of subfreezing glacier ices.

GL is without question a useful tool, but it does fail to describe significant strain rate variations that have been measured in the ice sheets. An unfortunate tuning coefficient called enhancement (E) is introduced as a multiplier of the stress term to describe these variations. E is quantitatively very important, in some instances varying by 1 order of magnitude. Three situations for which E is important are as follows:

1. E is significant in calculations of flow of the Greenland ice sheet and Canadian Arctic ice caps, at the scale of whole ice sheet models and at the scale of the ice divide regions which are particularly relevant to ice core studies. The lower portions of these ice bodies (consisting of ice deposited during the last ice age) are rheologically soft, with an average E relative to overlying Holocene ice of 2.5 [*Fisher and Koerner*, 1986; *Dahl-Jensen and Gundestrup*, 1987; *Paterson*, 1991].

2. E is used to describe the flow of dirty basal layers which have a high rock content. For example, E in such layers beneath Dye 3 and GISP2 are 4 and 7, respectively [*Dahl-Jensen and Gundestrup*, 1987; G.D. Clow and N. Gundestrup, unpublished data, 1997]. A most surprising yet uncontroversial measurement by *Echelmeyer and Zhongxiang* [1987] shows E=120 for a rock-rich ice beneath an alpine glacier (the Urumqi) in the Tien Shan. Even if they are thin, such extremely soft layers can contribute significantly to the overall flow of an ice mass [*Echelmeyer and Zhongxiang*, 1987].

3. E is used for analyzing the distribution of velocities across ice stream shear margins, for the purpose of learning basal characteristics and force balance partitioning for these ice streams. Estimates of E for the shear margins are as high as 12 [*Echelmeyer et al.*, 1994].

Laboratory experiments have conclusively shown [*Budd and Jacka*, 1989; *Jun et al.*, 1996] that a significant source of E is variations in ice crystal c axis fabric strength (fabric meaning the statistics of orientations). The dependence of viscosity on fabric strength is a consequence of the strong deformation anisotropy of single ice crystals [*Lliboutry and Duval*, 1985]. Deviations of fabric from isotropic can plausibly account for nearly a factor of 10 variation in E [*Shoji and Langway*, 1988; *Jun et al.*, 1996], and it is reasonable to suggest that this is the only important control on E in natural settings. *Paterson* [1991] reviewed all relevant data on the subject and concluded that crystal fabric variations cause most of the softening of the ice age ices, as noted above. Although this conclusion is probably sound, analyses of tilt of the Dye 3 borehole have shown that fabric cannot be the sole control [*Dahl-Jensen and Gundestrup*, 1987; *Paterson*, 1991]; a recent, detailed study strongly suggests that fabric effects account for no more than 70% of the E variations at Dye 3 [*Thorsteinsson et al.*, 1999].

Several analyses have shown that E variations in the ice sheets correlate strongly with rock particle content, chemical impurities, and crystal size [*Koerner and Fisher*, 1979; *Dahl-Jensen and Gundestrup*, 1987; *Fisher and Koerner*, 1986] and have suggested that these are a major control on E. In recent years, crystal size variations have been discounted for several reasons. First, *Jacka* [1984] has shown that crystal size evolves to an equilibrium value for a given strain rate and therefore is clearly a consequence of strain rate. This does not, however, mean this equilibrium value is independent of possible crystal size-dependent deformation mechanisms. Further, *Dahl-Jensen et al.* [1997] have shown that the equilibrium crystal size is not purely a function of strain rate but also of impurity content. Second, the apparent dominance of dislocation creep over grain boundary sliding and diffusional creep as the mechanism responsible for GL argued against a direct grain size dependence [*Duval et al.*, 1983]. Third, *Paterson* [1991] cites laboratory experiments on ices from Vostok [*Pimienta et al.*, 1988] and Dye 3 [*Shoji and Langway*, 1988]. As evidence against a grain-size-sensitive mechanism, these experiments are weak, primarily because both data sets contain a large range of crystal fabrics, whose effects could obscure a modest, but important, grain size dependence. Furthermore, most of these tests were conducted at stress levels much higher than those in ice sheets, which favors dislocation creep mechanisms [*Goldsby and Kohlstedt*, 1997]. Further, the Shoji and Langway analysis used inferred grain size rather than measured grain size (their Table III), except for their Figure 1, which shows a better correlation of E with grain size than with sonic velocity (a proxy for fabric strength).

Nonetheless, it is also true that none of the above provide convincing evidence in support of a grain size dependence either. Laboratory experiments have never demonstrated a grain size dependence at grain sizes and temperatures characteristic of the ice sheets [*Duval et al.*, 1983]. In addition, *Goldsby and Kohlstedt*'s [1997] experiments were conducted for extremely fine grains and low temperatures. Thus *Peltier*'s [1998] application of these experiments requires extrapolation over a large range of grain sizes and temperatures to obtain relations for terrestrial ice sheets.

Having discarded grain size from the list of strain rate controls, investigators have attributed residual E variations (those not ascribed to fabric variations) to chemical impurities and/or rock particles [*Paterson*, 1991; *Thorsteinsson et al.*, 1999]. Laboratory experiments have shown that single ice crystals become substantially softer if doped with acids (HF and HCl) that can substitute in the crystal lattice. One set of experiments examined the rheologic effects of an important natu-

ral salt, NaCl, and found that this impurity stiffens ice single crystals [*Riley et al.*, 1978]. The relevance of these studies to the ice sheets is unclear, as most impurities will be interstitial, if in the crystal, and the dominant acids in the ice sheets are sulphuric and nitric, and these are neutralized in the dust-rich ice age ices of Greenland. Further, impurities most likely segregate to grain boundaries [*Paren and Walker*, 1971]. Accumulation of impurities at grain boundaries would likely facilitate grain boundary-dependent deformation mechanisms like sliding and diffusion [*Holdsworth and Bull*, 1970; *Barnes et al.*, 1971; *Fisher*, 1987].

Studies of rheologic effects of dispersed rock particles have shown widely conflicting results (see review by *Budd and Jacka*, [1989]), with substantial stiffenings and softenings both reported at 10% volume. Some of this variation may be meaningful. If rock particles embedded in ice are surrounded by liquid films, they may act as soft inclusions because ice can negotiate them by regelation and boundary slip [*Echelmeyer and Zhongxiang*, 1987]. If no liquid is present, rocks will act as hard inclusions and stiffen the ice in a local region around each particle due to viscous effects [e.g. *Durham et al.* 1992] and due to interaction with dislocations [*Ashby*, 1969]. If grain boundary sliding is important, particles can stiffen the polycrystal by pinning grain boundaries [*Ashby*, 1980]. At concentrations high enough for particle-particle interactions to become important, stiffening most likely occurs [*Hooke et al.*, 1972], though the one observation of high E [*Echelmeyer and Zhongxiang*, 1987] in a frozen till with 60 to 70% rock content contradicts this in a spectacular fashion. Recent reviews of ice rheology have concluded that rock particles are unlikely to be significant at the low concentrations found in the ice sheets, with the possible exception of the dirty basal layers, for which a direct role of rock particles is a leading contender.

To discern the contributions to E of all these factors (fabrics, chemical and solid impurities, and crystal size), several complementary approaches are valuable. Laboratory experiments ("ice squeezing") have produced important results but have two difficulties. First, they are generally conducted at stresses higher than those of interest in the ice sheets. This is a particular problem in view of *Goldsby and Kohlstedt*'s [1997] claim that while dislocation creep dominates at high stresses, grain-boundary sliding becomes important at lower stresses typical for glaciers and ice sheets. Thus the experiments of *Duval and LeGac* [1980] and *Jones and Chew* [1983], which show no grain size dependence at stresses of 0.5 MPa and higher do not resolve this issue. Second, laboratory experiments on polycrystals do not control the crystal fabric and the grain size. The difficulty this causes for interpretation is illustrated by the study of *Dahl-Jensen et al.* [1997]. In the course of their experiments, crystal size and fabric continually evolved, rendering the final ice textures rather different from the original. It would be desirable to determine an instantaneous strain rate at the beginning of such experiments, but this would raise serious questions concerning possible annealing of ice samples.

Thus in situ deformation studies, such as analyses of tilt of the deep boreholes in the ice sheets, are extremely valuable, despite the fact that stress is inferred, not measured. The results of these studies have not, however, been generally diagnostic because variations in enhancement, fabric, most impurities, and crystal size are strongly correlated (high-enhancement ices generally having strong fabrics, high rock and ion contents, and small crystals).

The study presented here is an in situ ice deformation study. Following *Holdsworth and Bull* [1970], we excavated a tunnel through basal layers of Meserve Glacier, an alpine glacier in Wright Valley, Antarctica. The basal layers of this glacier have a high but variable impurity content [*Holdsworth*, 1974]. Many of these impurities appear to be derived from entrainment of bed material [*Cuffey et al.*, 2000]. The strength of correlations between candidate rheologic controls here is therefore much weaker than in the ice age ices of the ice sheets, providing a fresh perspective on this old problem. The fabric strength is also much more uniform here than in the ice sheets, with most ices of the basal Meserve having a very well developed single maximum normal to the planes of shear [*Anderton*, 1974]. Total ion contents in the Meserve basal ices average 200 μmol L^{-1}, a factor of 20 greater than the dirtiest ice age ices from Greenland, but vary over a huge range, from 35 to 880 μmol L^{-1}.

The goal of this study is to propose a simple empirical model for E variations due to variations in crystal size and ionic and solid impurities, and to use measurements of strain rate and ice properties for Meserve glacier ices to constrain model parameters. The results obtained here are essentially for one temperature (-17°C) and one stress ($\sim 5 \times 10^4$ Pa). These conditions are important ones for many glaciologic problems. *Cuffey et al.* [this issue] explore the applicability of the resulting calibrated model to the ice sheets.

2. A Semiempirical Model

2.1. General Approach

We assume that the softening effects of grain size and impurities can be represented by a scalar coefficient (E_*) that multiplies a second rank tensorial function ($\dot{\boldsymbol{\epsilon}}^{\mathrm{F}}$) of crystal fabric and stress (an "anisotropic flow law" for clean polycrystalline ice which becomes equivalent to the GL for an isotropic fabric):

$$\dot{\boldsymbol{\epsilon}} = A(T)\; E_*\; \dot{\boldsymbol{\epsilon}}^{\mathrm{F}}\left(\boldsymbol{\tau}, \boldsymbol{S}\right), \tag{1}$$

where $\dot{\boldsymbol{\epsilon}}$ is strain rate, A is the strongly increasing function of temperature inferred from numerous studies and compiled by *Budd and Jacka* [1989] and *Paterson* [1994], $\boldsymbol{\tau}$ is the deviatoric stress tensor, and $\boldsymbol{S}$ is a tensorial de-

scription of crystal fabrics such as the average Schmid tensor [*Azuma and Higashi*, 1985; *Alley*, 1988]. The primary goal of the analyses that follow is to constrain E_*. A "true" E_* is almost certainly a function of temperature, but we have no capacity to resolve temperature dependence here. A in this study will be a constant coefficient for the temperature at which strain rates were measured (≈-17°C).

We also are not proposing here any additions or alterations to $\dot{\epsilon}^F$ relative to the proposals for it in the literature. We follow *Thorsteinsson et al.* [1999] in considering two end-member views of the function $\dot{\epsilon}^F$: the Azuma model [*Azuma*, 1994; *Azuma and Goto-Azuma*, 1996], which assumes uniform strain rate throughout the polycrystal, and the Sachs model which assumes uniform deviatoric stress [*van der Veen and Whillans*, 1994; *Thorsteinsson et al.*, 1999].

2.2. The New Term

In proposing a form for E_* we are guided by the following considerations:

1. Algebraic and conceptual simplicity are required.
2. Following *Barnes et al.* [1971] and *Goldsby and Kohlsted* [1997], we suppose that bulk strain rate is due to a sum of grain-size-dependent and grain-size-independent mechanisms.
3. We allow that the dependence of E_* on ion content may be nonlinear, due to lattice saturation effects (e.g., the laboratory experiments of *Nakamura and Jones* [1970] showing sublinear dependence) or due to nonlinear dependence on the grain boundary ion content (e.g., the strain rate mechanism could depend on the grain boundary thickness in a nonlinear fashion, and this thickness may be proportional to bulk ion concentration).
4. Rock particle content may correlate with strain rate for two separate reasons: (1) because particles affect viscosity directly, and (2) because a certain fraction of the measured bulk ion content derives from rock surface interfacial films [*Dash et al.*, 1995; *Cuffey et al.*, 1999] or the rock surface itself. This fraction of the ions is not residing in grain boundaries or within the crystal lattice and therefore does not directly affect the viscosity of ice with widely scattered mineral particles.

The class of models we explore describes variations of E_* relative to its mean ($\langle E_* \rangle$) as

$$\frac{E_*}{\langle E_* \rangle} = E_{*D} E_{*C} + \beta V_r, \tag{2}$$

where E_{*D} and E_{*C} are enhancements associated with variations of grain size and chemical impurity content, respectively. The term βV_r describes a direct softening effect of fractional rock volume V_r (volume of rock per volume of ice) according to a single constant β. The dependence on V_r was kept strictly linear for simplicity, which appears reasonable as the highest V_r values are only ≈ 0.02.

We define

$$E_{*D} = (1 - \tilde{\omega}) + \tilde{\omega} D^{-m}. \tag{3}$$

Here D is the average grain size (diameter in mm), m is a constant (found, but not forced, to be positive), and $\tilde{\omega}$ is a number between 0 and 1, inclusive, which indicates the relative magnitude of the size-dependent component to the size-independent component. If $\tilde{\omega} = 0$, there is no grain size dependence at all, whereas if $\tilde{\omega} = 1$, the grain size dependence is pervasive. An alternative description of E_{*D} which differs only by a constant multiple (and therefore is equivalent in the present context) is

$$E_{*D} = 1 + \omega D^{-m}, \tag{4}$$

for which

$$\omega = \frac{\tilde{\omega}}{1 - \tilde{\omega}}. \tag{5}$$

This alternative trade-off parameter ω varies from 0 to ∞, corresponding to $\tilde{\omega} \in [0, 1]$. We henceforth use ω because it enables a detailed look at the limiting behavior as $\tilde{\omega}$ approaches its upper and lower limits via log-log plots. Normalizing to the constant $\langle E_* \rangle$ indicates that we do not know the value for $\tilde{\omega}$ in the standard compilations for flow law prefactors A [*Budd and Jacka*, 1989; *Paterson*, 1994].

We define the chemistry-dependent factor as

$$E_{*C} = 1 + \sum_i \gamma_\lambda^i C_i^\lambda \left(1 + \eta A_r\right)^{-\lambda}. \tag{6}$$

This describes enhancement by ions $i = \mathrm{SO_4}, \mathrm{Cl}, \cdots$ of bulk measured concentration C_i, according to a simple power relation with exponent λ and prefactors γ_λ^i. The inferred prefactors not only depend on the ion considered but also necessarily on the nonlinearity λ. The notation γ_λ is therefore used to indicate which λ corresponds to a given coefficient γ.

We have measurements of nine ions. Using all nine ions in the sum would not produce meaningful results, as many of the ions are strongly correlated. Typically, we use only three ions, which are representatives of strongly correlated ion groups. These are $\mathrm{SO_4}$, Cl, and inferred acidity (denoted by plus), so, for example, the factor E_{*C} is

$$1 + \left(\gamma_1^{\mathrm{SO_4}} C_{\mathrm{SO_4}} + \gamma_1^{\mathrm{Cl}} C_{\mathrm{Cl}} + \gamma_1^{+} C_{+}\right) \left(1 + \eta A_r\right)^{-1} \tag{7}$$

in the case of a linear dependence on concentration (λ=1).

The fractional reduction of measured ion content to account for storage on/in rocks depends on a constant η (units of length) and the measured area of rock per volume of ice (A_r). We choose to represent this fractional reduction using a divisor $(1 + \eta A_r)$ rather than a coefficient $(1 - \eta A_r)$ because the divisor ensures there will be no change of sign at large A_r. In the analyses we have tried both and found that it makes little difference.

The multiplicative form of equation (2) implies that ions will act to enhance grain-size-dependent deformation mechanism(s), for example by facilitating grain boundary sliding. Such an interaction is likely for two reasons. First, most ions in the crystal interior will be interstitial and thus have no rheologic effects. Second, the concentration of ions in grain boundaries is likely very much higher than the concentration of ions in the crystal interiors [*Paren and Walker*, 1971; *Alley et al.*, 1986]. Below, we justify the multiplicative form by showing that models for which grain size and ions are only separate, additive terms in E_* provide a significantly worse fit to the data.

3. Analysis of Meserve Glacier Data

We use measurements of ice properties and in situ strain rates to find best fit values for free parameters in equation (2) using standard geophysical inverse procedures.

3.1. Tunnel and Measurements of Strain Rates

In the austral summer of 1995-1996 we excavated a 20-m-long tunnel into the basal layers of Meserve Glacier on the northeast margin beside the *Holdsworth and Bull* [1970] camp (Figure 1). The tunnel was ~ 2 m high and ~ 1 m wide. It was excavated with chain saws, pick axes, and shovels. The tunnel entered the glacier normal to the marginal cliff and curved up-slope to parallel the flow line (Figure 1).

We excavated two alcoves (~0.7 m in depth, ~1.2 m wide, ~2.0 m high) for the strain rate measurements, one at 8 m from the tunnel entrance, and the other at 16 m. The rear walls of these were smoothed, and regular arrays of metal bolts were frozen into place in drill holes. The plane of the grid at 8 m (hereinafter referred to as the D grid (downflow)) was angled ~10°from the flow line and was positioned to take advantage of prominent layering of the stratigraphy, seen as three bands of "amber"-colored rock-particle-rich ice amidst white, bubbly, clean ice. The plane of the grid at 16 m (hereinafter referred to as the U grid (upflow)) was parallel to the flow line and had a simpler stratigraphy, with one prominent amber layer.

The D grid had 18 horizontal rows of bolts, spaced 0.1 m apart vertically, and three columns, separated by 0.1 m. The U grid had 17 horizontal rows of bolts and three columns, with similar separations. Distances between neighboring bolts were measured with micrometers, once in late December 1995, once in late January 1996, and once in December 1996. We calculated strain rates from changes in relative bolt positions, using standard techniques (E.D. Waddington and L.A. Rasmussen, unpublished manuscript, 1993), yielding 17 measurements of strain rates at the D grid and 16 at the U grid, each with a redundancy of four. Inferred strain rates using the January 1996 and December 1996 positions relative to the December 1995 positions are nearly identical, indicating that the measurement error is very small relative to the signal (for shear strain rates) and

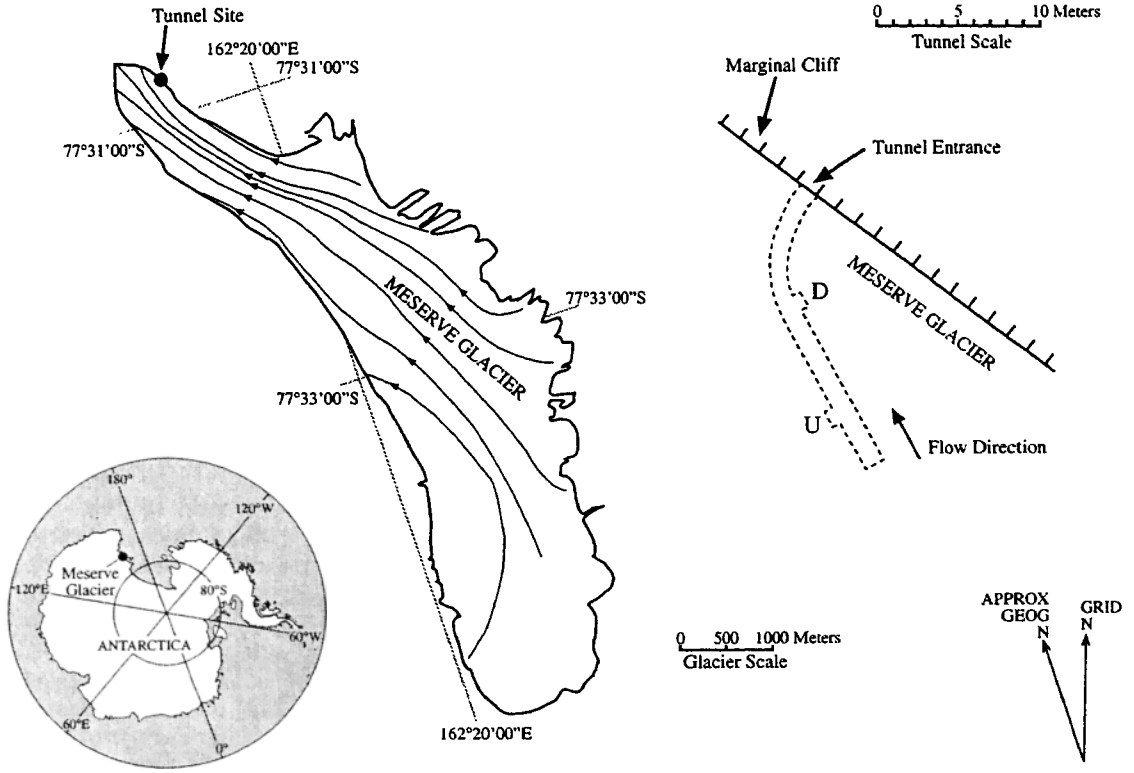

Figure 1. Map of Meserve Glacier, modified from *Holdsworth* [1974, Figure 2], showing location of the glacier, location of the tunnel, the tunnel plan, and the location of the strain grids.

that no measurable temporal change of the strain rates occurred.

3.2. Ice Sampling

Using chain saws, we extracted six vertical columns of ice from the tunnel walls, from 7.0, 7.5, 9.5, 10.5, 11, and 16.5 m from the tunnel entrance. Ice from these was used for chemistry, particle, and density measurements and to make thin sections.

3.2.1. Chemistry. Complete vertical profiles of major ion content were obtained for the 16.5 and 9.5 m columns and for a vertical profile through the amber-layer banding and adjacent white ice at 7.5 m. Columns were subsampled at 3 to 4 cm resolution in the stratified portions and at 10 cm resolution in the upper white ices. Concentrations of major ions (Na, K, Mg, Ca, NH_4, Cl, NO_3, SO_4) for these samples were obtained by ion chromatography at the University of New Hampshire glaciochemistry laboratory using standard, stringent cleaning and filtering procedures [*Buck et al.*, 1992; *Mayewski et al.*, 1997]. Average charge imbalance was 5% (missing negative charges, likely bicarbonate). Samples with missing positive charge were few, except for those from the upper portion of the 9.5 m profile. where ~5% positive charges were missing. We assume these to be H^+.

Repeat measurements on the same samples revealed a very high reproducibility of chemistry measurements (to within a few percent). A few samples were run without immediately filtering rock particles, and these had up to 10% higher ion contents. Rock particles were immediately filtered for all the measurements used here.

3.2.2. Particles. Twins of all samples for chemistry analysis were saved and weighed, and rock mass fraction was determined by melting, filtering, drying and weighing (filter pore size was 2.5 μm). Subsequently, particles were resuspended and agitated, and grain size distributions were measured using a laser light scattering and extinction instrument (the Model 770 AccuSizer of Particle Sizing Systems, Santa Barbara, California, operated by the Batelle Pacific Northwest Laboratory, Richland, Washington). Particle size distributions were found to be quite consistent throughout the amber ices, with a mean size of ~0.2 to 0.7 mm, as found by *Holdsworth* [1974]. An estimate of rock surface area per volume of rock was made for each sample by approximating the particles as spheres.

3.2.3. Void fraction. Prior to melting to extract rock particles, we measured the "twin" samples' density, using an isostatic weighing procedure. Void fraction was then estimated from these bulk density measurements, the rock mass measurements, and an assumed density for ice crystals (920 kgm^{-3}) and for rocks (2650 kgm^{-3}).

3.2.4. Thin sections. We prepared thin sections from the ice columns using standard procedures (separating ice slices with a band saw, smoothing one surface, affixing it to transparent plates using freeze-on and/or glue and reducing the ice to submillimeter thickness). The rock-rich amber ices presented a special challenge. The smoothing and thinning of amber ice slices was done with sand paper with various grit sizes (finer grit being used toward the end of the task); abrasion and chipping rapidly destroyed metal blades, necessitating this more laborious task of sanding. Before freeze-on, visibly protruding rock particles were plucked from the surface to ensure a smooth contact. A total of 45 horizontal thin sections plus 14 vertical plane sections were prepared.

3.2.5. Crystal size. Each of the 45 thin sections was photographed under crossed polarizers and crystal size measured from the photographs using the linear intercept method. Randomly oriented and positioned lines were drawn across the photographs and number of grain intersections counted. The average length per grain was multiplied by 1.5 to approximate the crystal diameter [*Underwood*, 1970]. The number of grain intersections for each measurement was at least 90 (in the coarser ices) and as great as as 200 (in the fine ices). The resulting average length per grain was reproducible to within ± 0.06 mm, based on triplicate measurements for each thin section.

In the vertical plane thin sections the variability within white and amber ice strata was seen to be much smaller than the variability between strata. However, the boundaries between some amber layers and white layers showed pronounced interlayering of fine and coarse grains. The average grain size of these regions is thus intermediate between those for the bounding layers. The corresponding uncertainty on average grain size for given intervals of the strain grids is part of the total $\pm 20\%$ uncertainty used in our statistical analyses (see below).

The grain sizes reported here refer to grain size seen in horizontal planes. The grains are somewhat flattened, with vertical dimension being 0.7 to 0.9 of the horizontal dimension [*Anderton*, 1974].

3.2.6. The *c* axis fabrics. We calculate $\dot{\epsilon}^F$ directly from *c* axis fabric data (Appendix A) and assumed stress tensors according to two different end-member "anisotropic" relations and two different end-member views of the stress state near the tunnel. Two free parameters (e_{AS} and e_T) which vary from 0 to 1, inclusive, are introduced to describe the trade-off between end-members of these spectra (anisotropic model and stress model, respectively). The potential for *c* axis fabric variations to dominate variations in strain rate [*Jun et al.*, 1996] makes this a very important part of the analysis. However, *c* axis fabrics proved to have little effect on results presented henceforth due to the low variability of fabric strength at the study site, and we were unable to constrain e_{AS}. A detailed discussion is thus postponed to Appendix A.

3.3. Analysis Method

3.3.1. Common reference frame. To interpret strain rate variations in terms of measured and derived ice properties, it is first necessary to compile all data

in one common spatial reference frame. For this we use the thirty-three 0.1 m vertical intervals corresponding to the strain rate measurements (see Appendix B).

All the final data used in the analyses are shown in Figure 2, after translation to the common reference frame, and single-value reproducibilities are listed in the caption. Table 1 lists minima, means, and maxima for all these parameters. The c axis fabric data derived from many of the thin sections are shown in Appendix A.

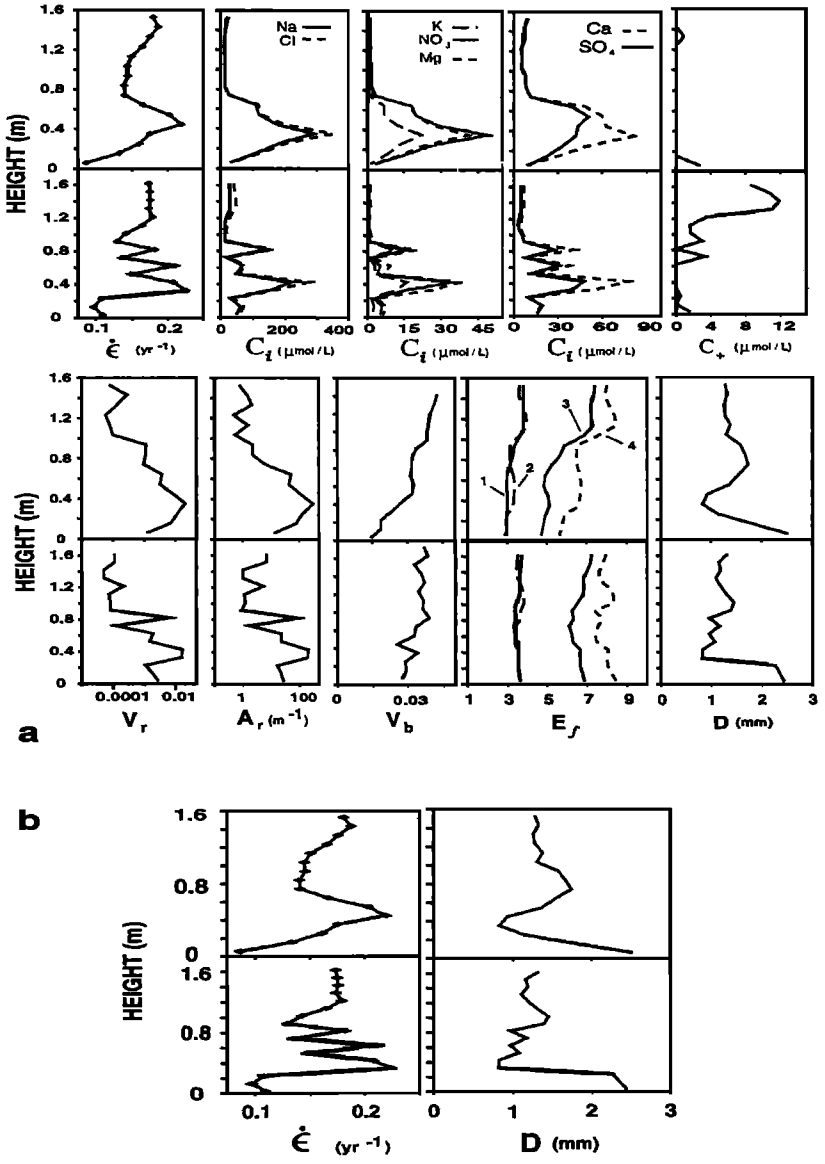

Figure 2. Measured strain rates and all data used in the viscosity analysis. (a) all the data. (b) reproduction of just the strain rate and grain size data. Top (bottom) of each panel is U grid (D grid) data. All variables are as in the text, except E_f which is the enhancement of downflow shear relative to isotropic ice, calculated from (1) uniform stress model without tunnel stresses, (2) uniform stress model with tunnel stresses, (3) uniform strain rate model without tunnel stresses, and (4) uniform strain rate model with tunnel stresses. Height refers to height above base of the strain grid, which is 20 cm (40 cm) above topographic crests of the ice/substrate interface at the U grid (D grid). (The substrate here is frozen till, and we mapped its topography in detail along the tunnel wall flow lines. Its roughness has an amplitude of approximately 20 cm.) Uncertainties on single measurements, as determined by repeat measurement of samples, are approximately ± 1.5 μmol L^{-1} for ions (increasing to ± 3 μmol L^{-1} in the most impure samples), ± 0.003 for V_b, and ± 0.06 mm for D. Uncertainty on the E values results primarily from uncertainty of the thin section orientations and is approximately $\pm 10\%$. Uncertainty on single measurements of the rock content were estimated not from repeat measurements on the same sample but from measurements on adjacent samples in the same stratigraphic layers and are approximately $\pm 15\%$ in the amber ices.

Table 1. Summary of Measured Ice Properties in Meserve Basal Ices[a]

Property	Minimum	Mean	Maximum	Units
C_{Na}	11.8	65.1	291	μmol L^{-1}
C_{NH_4}	0.07	0.44	1.28	μmol L^{-1}
C_K	0.27	3.98	22.3	μmol L^{-1}
C_{Mg}	0.73	8.80	41.1	μmol L^{-1}
C_{Ca}	3.90	22.5	81.4	μmol L^{-1}
C_{Cl}	12.1	76.1	353	μmol L^{-1}
C_{NO_3}	0.41	8.40	49.3	μmol L^{-1}
C_{SO_4}	2.49	17.0	51.0	μmol L^{-1}
C_T	37.3	202.3	881	μmol L^{-1}
C_+	0.00	1.30	11.9	μmol L^{-1}
V_b	0.014	0.033	0.043	
V_r	5×10^{-5}	3.3×10^{-3}	0.021	
A_r	0.50	41.4	308	m^{-1}
E_A	4.70	6.30	7.42	
E_S	2.93	3.43	3.82	
$E_{A,T}$	5.64	7.45	8.46	
$E_{S,T}$	2.87	3.48	4.00	
D	0.81	1.40	2.51	mm

[a] C_T is the total ionic content. E_A, E_S, $E_{A,T}$ and $E_{S,T}$ are shear enhancements relative to isotropic ice calculated according to Azuma and Sachs (A and S) with and without tunnel closure stresses (T indicates such stresses are included). All other variables as defined in text.

The data (Figure 2) show strong correlation of strain rate with both chemical impurities and with grain size. For the D grid there are three prominent strain rate maxima between 0.3 and 0.8 m, a minimum at 0.9 to 1.0 m, and high values again in the upper 0.4 m. The three maxima correlate strongly with chemical and rock impurities (and visually with amber ice layers), the correlation being best for SO_4 and Ca. In other respects the impurities do not correlate with strain rate whereas grain size does. Inverse grain size clearly has the minimum at 0.9 to 1.0 m and high values for the 1.2-1.6 m interval relative to the 0-0.25 m interval. Both of these features are much larger than the 0.06 mm reproducibility of the thin section data. In the grain size data the variations between 0.3 and 0.8 m corresponding to the three rapidly straining layers are unquestionably real; thin sections show unambiguously that the impure layers have D in the range 0.6 to 0.9 mm, whereas the pure interlayers have D in the range 1.1 to 1.5 mm. These variations are here muted because 0.1 m intervals from 0.5 to 1 m are an average of pure and impure layers of varying proportions. The D variations between 1.2 and 1.7 m are less meaningful; here there is obviously some stratification in the ice according to the thin section data, but this was not visible due to the low impurity content and therefore we cannot assign weighted averages as we did for the lower layers where stratification is visually prominent.

Note that there is a slight increase of chemical content from 1 m to the top of the profile. This small increase is completely out of proportion to the increase of strain rate, relative to variability in the rest of the profile. A possibility, though, is that this small increase of chemical content is sufficient to cause smaller grain sizes.

For the U grid, there is a pronounced strain rate maximum at 0.5 m, a minimum at 0.8 m, and a significant rise toward the top of the profile. All these features are seen also in the grain size data. In contrast to the impurities, the minimum at 0.8 m and the relative values between top and bottom of the profile are clearly seen in the grain size data (inversely). Impurity content is high in the rapidly straining layer at 0.2 to 0.65 m. Note that the maximum corresponds to the maximum of sulphate rather than chloride.

3.3.2. Inversion procedure. Our task is to find values for the free parameters in equations (2) and (A8) that best describe the measured strain rates in terms of the data in all the other panels of Figure 2. This is only a meaningful exercise if the model variables vary independently to some extent. Figure 3 shows correlations of the most important ice properties. This diagram is encouraging; in contrast to the ice age ices of the ice sheets, here there is significant independent variation of crystal size, ionic content (Figures 3c and 3d), fabric enhancement (Figures 3g and 3h), and rock content (Figure 3f). Sulphate and chloride vary independently to a significant degree (Figure 3a). On the other hand, rock surface area and volume are very strongly correlated (Figure 3e), suggesting it will be difficult to separate direct rheologic effects of rock particles from "ion storage" effects. The ions fall into several distinct groups, within which the correlation is very strong (Figure 2). These groups are the sulphate group (SO_4 and Ca), the chloride group (Cl and Na), the nitrate group (NO_3, K, Mg), unbalanced positive charges (presumed acidity and denoted by plus), and ammonia (NH_4). Further, the nitrate and chloride groups correlate strongly in the amber ices and therefore are difficult to treat separately. Ammonia occurs at very low concentrations and is not correlated with strain-rates, so we will not consider it further.

Free parameters in the strain rate model that we wish to optimize are A, ω, m, γ^{SO_4}, γ^{Cl}, γ^+, λ, η, β, e_{AS}, and e_T. In optimizations for which all these parameters are free, 22 degrees of freedom remain. We define a chi-square performance index in terms of observed and modeled strain rates ($\dot{\epsilon}^o$ and $\dot{\epsilon}^m$):

$$\chi^2 = \sum_{i=1}^{33} \frac{(\dot{\epsilon}_i^m - \dot{\epsilon}_i^o)^2}{(\sigma_\epsilon^2 + \sigma_P^2)_i}, \tag{8}$$

where σ_ϵ is the variance of measured strain rates and σ_P is the variance in predicted strain rate due to uncertainties of all input parameters.

Optimal model parameters are those for which χ^2 is minimized. We perform the minimization using iterative application of singular value decomposition. This

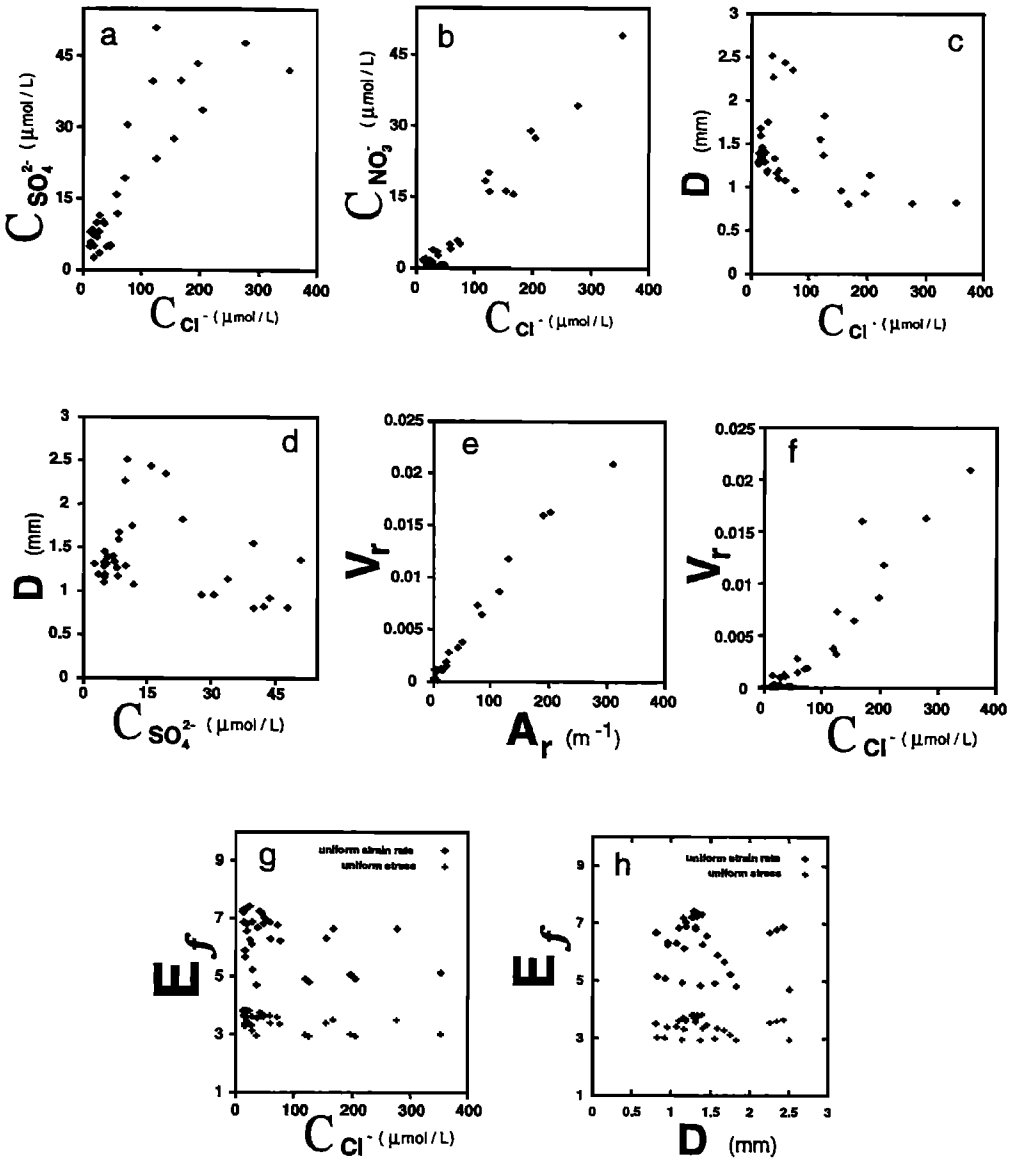

Figure 3. Covariation of many of the variables shown in Figure 2.

was supplemented with "shaking" (forced arbitrary changes of parameters, as in simulated annealing procedures [e.g., *Press et al.*, 1992, p. 436] to allow escape from local minima which were found to exist in some regions of the parameter space.

We used a preliminary solution (which proved to be very close to the final solution) to calculate σ_P. We estimated, based on reproducibility of measurements and on ambiguity in the interpolating and partitioning procedures, that a reasonable, modestly conservative, error for values of most input parameters is ±20%. We then used a Monte Carlo procedure to generate 80 separate strain rate predictions, forcing each input parameter to be perturbed by uniform random variables between ±20%, generated using the Matlab random number generator; σ_P is the variance of the resulting strain rate predictions (Figure 4) at each grid point (which are very nearly normally distributed). Average values for σ_ϵ and σ_P are 2% and 7% of the measured strain rates, respectively.

Confidence intervals for model parameters were defined, according to standard procedure, by isolines of $\Delta\chi^2 = \chi^2 - \chi^2_{\min}$, which is the decrease of model performance relative to that for the optimal model ($\chi^2_{\min}$ being χ^2 for the optimal model). The most accurate method for identifying the $\Delta\chi^2$ value corresponding to a given confidence probability is Monte Carlo simulation [e.g., *Menke*, 1989; *Press et al.*, 1992]. By this method, each of the simulated strain rate "data sets" resulting from random perturbation of input parameters is treated as true data, and an optimal model is found for each. The resulting distribution of optimal model parameters directly gives the confidence intervals, if a sufficient number of simulated data sets is used.

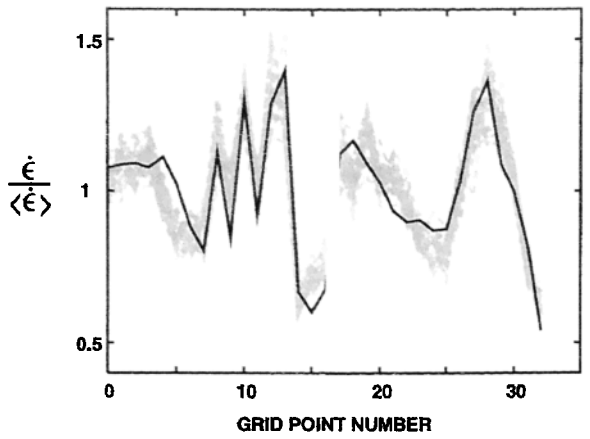

Figure 4. Measured strain rates (solid line) for all 33 grid points (corresponding to the measured strain rates) used in the rheology analysis, plus 30 of the recalculated strain rates based on randomly perturbed input parameters. Strain rate is shown normalized to mean.

If errors are normally distributed and the model can be approximately linearized within the confidence limits, then $\Delta\chi^2$ is distributed as a χ^2 variable, which allows a much quicker identification of the $\Delta\chi^2$ corresponding to a given confidence level. Here we use this latter approximation but have performed some Monte Carlo simulations to show that the approximation is a good one and that the global confidence limits are accurate (Figure 10).

We utilize the χ^2 approximation as described by *Press et al.* [1992, pp. 688-693]. For a total number of model parameters M, a combination of fixed parameters, μ in number, is statistically acceptable (i.e., within the global confidence limits) if $\Delta\chi^2$ after optimizing the $M-\mu$ nonfixed parameters is less than χ^2 with μ degrees of freedom. Thus this statistical method explicitly evaluates the relative merits of models with differing numbers of free parameters, as long as the models with fewer free parameters are a subset of the most complete model.

A really unacceptable model is one that can be rejected with 99.5% confidence. We define an index of poor fit $\mathcal{P}_{0.995}$ in terms of a model's $\Delta\chi^2$ and the $\Delta\chi^2$ for rejection at 0.995 probability ($\Delta\chi^2_{0.995}$) as

$$\mathcal{P}_{0.995} = \frac{\Delta\chi^2}{\Delta\chi^2_{0.995}} - 1. \quad (9)$$

Models with $\mathcal{P}_{0.995} > 0$ can be firmly rejected. We define a similar index relative to 95% confidence as

$$\mathcal{P}_{0.95} = \frac{\Delta\chi^2}{\Delta\chi^2_{0.95}} - 1. \quad (10)$$

Models with $\mathcal{P}_{0.95} < 0$ are acceptable at this confidence.

4. Results

4.1. Optimal Models

The optimal model incorporating 11 free parameters (Table 2) has χ^2=23.0, which is comparable to the degrees of freedom (22), indicating the model is generally adequate (Figure 5), though not spectacular. A sparser model (Table 2) with five free parameters (ω, m, γ^{SO_4}, γ^+, η) is nearly as acceptable (χ^2=32.7 for 28 degrees of freedom), indicating that the grain size and ionic parameters are dominant in determining the optimal model. Variations of crystal size and chemical content dominate strain rate variations at the study site (Table 3). The importance of both variables is directly apparent qualitatively (Figure 6) from the data in Figure 2 and the optimal model parameters.

Both optimal models have $\omega = \infty$, corresponding to $\tilde{\omega} = 1$. Thus there is a simple proportional correlation of strain rate and grain size of the form $E_{*D} \propto D^{-0.6}$. In addition, there is a linear or weakly nonlinear dependence on ionic content. Thus the large range of concentrations at the study site induces significant variations in strain rate here.

4.2. Necessity of Grain Size and Ion Dependencies

The only acceptable models are those for which both grain size and ions are important. We have experimented with all plausible models for which, in addition to stress and fabric, only rocks are important (m=0, γ^i=0), only ions are important (m=β=η=0), only rocks and ions are important (m=0), only grain size is important (γ^i=β=η=0), or only grain size and rocks are important (γ^i=0). All these models are rejected at >99.5% confidence; the associated combinations of fixed parameters fall well outside the 99.5% confidence limits. Pure grain size models have $\mathcal{P}_{0.995}$ in the range 1.9 to 2.2, pure ion models have $\mathcal{P}_{.995}$ in the range 5 to 9,

Table 2. Summary of Optimal Model Parameters for Full and Reduced Models

Parameter	Optimal Value	95% Confidence Interval
	Full Model	
e_T	0.0	[0, 0.6]
e_{AS}	0.2	[0, 0.92]
$\tilde{\omega}$	1.0	[0.17, 1.0]
m	0.64	[0.46, 2.2]
λ	1.53	[0.48, 3.7]
$\gamma^{SO_4}_{1.53}$	2.0×10^{-3}	$[1.3, 3.2] \times 10^{-3}$
$\gamma^{Cl}_{1.53}$	-9.7×10^{-5}	$[-17, 2] \times 10^{-5}$
$\gamma^{+}_{1.53}$	5.3×10^{-3}	$[1.1, 10.] \times 10^{-3}$
η	1.9×10^{-3}	$[-0.2, 8.5] \times 10^{-3}$
β	1.9	[-22, 8.3]
	Reduced Model	
$\tilde{\omega}$	1.0	
m	0.60	
$\gamma^{SO_4}_1$	0.019	
γ^{+}_1	0.09	
η	7.3×10^{-3}	

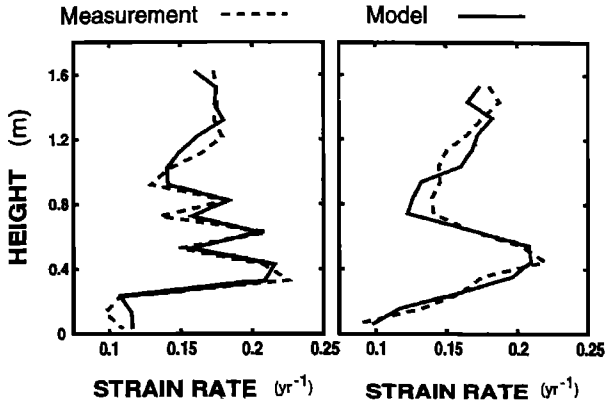

Figure 5. Model and measured strain rates for (left) the D grid and (right) the U grid. The model shown here is optimal.

pure rock models have $\mathcal{P}_{0.995}$ in the range 7 to 8, and mixed ion-rock models have $\mathcal{P}_{0.995}$ in the range 4.5 to 9. The corresponding $\Delta\chi^2$ are ~50 for the pure grain size models and 85 to 165 for the others. With reference to Figure 4, a model with $\Delta\chi^2 = 50$ has each point, on average, worse than the optimal model by twice the width of the gray zones.

4.3. Evidence Against an Additive Model

An alternative to equation (2) is the class of models in which effects of grain size and ions are additive

$$\frac{E_*}{\langle E_* \rangle} = 1 + \omega_a D^{-m} + \sum_i \gamma_\lambda^i C_i^\lambda (1 + \eta A_r)^{-\lambda} + \beta V_r, \quad (11)$$

where ω_a is the parameter equivalent to ω of the multiplicative model. These additive relations do not fit the data as well (Figure 7), for all values of ω_a. This justifies the multiplicative relation between ions and grain size in equation (2). However, the strength of this result is modest and this issue should be revisited in future analyses.

Table 3. Relative Significance of Ice Properties in Controlling Strain Rate Variations in the Meserve Glacier Basal Layers[a]

Rank	Property	Relative Contribution
1	crystal size	1.00
2	principal ion(s)	0.54
3	crystal fabrics	0.24
4	particles (ion storage)	0.23
5	acidity(?)	0.15
6	particles (direct effect)	0.00

[a]These rankings were calculated by removing each property from the optimal model and recording the increase of model-measurement mismatch. The relative magnitudes of these mismatch increases are the relative contributions reported here.

4.3. Grain Size Dependence

We find that strain rate depends on the inverse of crystal diameter to a power m in the range 0.5 to 0.75 as a bulk average (corresponding to the limit $\omega \to \infty$ or $\tilde{\omega} = 1$; Figure 8). Two alternative end-member interpretations of this average dependence (Figure 8) are that (1) there is a grain size-dependent deformation mechanism that dominates bulk viscosity and which has a low value for m (≈ 0.6); and (2) there is a grain size-dependent deformation mechanism depending strongly on grain size (m in the range 1.3 to 2.2) but whose total contribution to deformation is less than that of size-independent mechanisms (at $D = 1$ mm). Intermediate cases are admissible. With the present data we cannot discern which of these is correct (i.e., we cannot constrain ω). However, we can conclude that the D-dependent component is at least 15% as large as the D-independent component (Figure 9) at 95% confidence. We have confirmed the validity of confidence intervals on m directly using Monte Carlo simulations (Figure 10).

4.4. Role of Ions

4.4.1. Which ions are the most effective softening agents? To determine which ions are the most effective softening agents, we determine how well the strain rate variations can be explained given various assumptions about which ions cause the softening and what their relative γ values are. After having established that SO_4 or Ca produce the best results, we investigate γ^i for other ions as follows. Suppose that softening results from SO_4, from one other principal ion i, and from C_+. Then the ionic sum in equation (2) is $\gamma_\lambda^{SO_4} C_{SO_4}^\lambda + \gamma_\lambda^i C_i^\lambda + \gamma_\lambda^+ C_+^\lambda$. Further, require γ^i to be positive (γ^{SO_4} is positive too, but this is a result of the optimization). Then fix the relative sensitivity of the two ions at some ratio γ^i/γ^{SO_4}, optimize all other parameters, and compare the model mismatch to that for the optimal model. Because the ratio γ^i/γ^{SO_4} varies from 0 to ∞, it is easiest to define a new variable, R^γ, that ranges from 0 to 1 as

$$R_{a-b}^\gamma = \frac{\gamma^a/\gamma^b}{1 + \gamma^a/\gamma^b}, \quad (12)$$

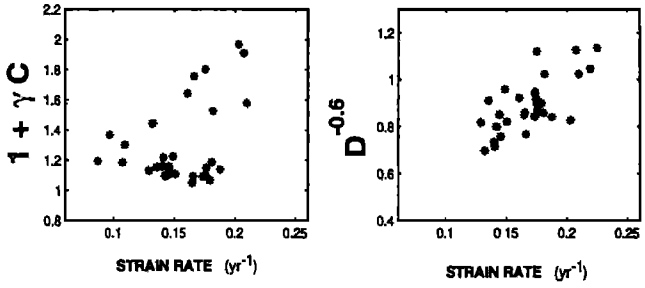

Figure 6. Correlation of measured strain rate with $1 + \gamma_1^{SO_4} C_{SO_4}$ and with $D^{-0.6}$, for all 33 grid points. This demonstrates that strain rate depends on both C and D.

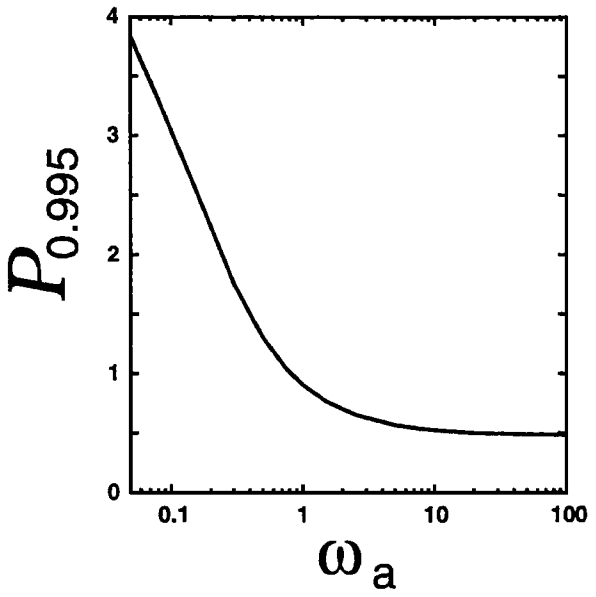

Figure 7. Poor fit index for purely additive models. All models with $\mathcal{P}_{0.995} > 0$ are rejected with 99.5% confidence.

which has a value 0.5 when the two γ are equal. Results for such experiments suggest (Figure 11) that sulphate and calcium are the most important softening agents, on a per molar basis, and that Na and Cl are unlikely to cause a per molar softening larger than 1/5 of that due to SO_4 or Ca.

4.4.2. Magnitude of ionic softening. Ion content variations in Meserve ice are large and cause significant variations of strain rate here. However, the factor of 20 variation in ion content causes less than a factor of 2 variation in strain rate. Thus the sensitivity of strain rate to ion content is rather low at these stress and temperature conditions. The enhancement E_{*C} due to a one micromolar concentration is $1+\gamma^{SO_4}$, which is not more than 1.3 and most likely is <1.05 (Figure 12). At the Meserve study site the inferred ionic softening corresponds to an average enhancement of $\sim 1 + \gamma_1^{SO_4} C_{SO_4} = 1 + (0.02)(20) = 1.4$. These results do not change if ions or combinations of ions other than SO_4 are used; to a good approximation the inferred sensitivity γ_λ^i is reduced in proportion to the ratio of concentrations $(C_{SO_4}/C_i)^\lambda$. Note that inferred γ_λ varies strongly with λ (Figure 12).

A direct inference from these results is that a 2 μM concentration of sulphate plus chloride (a quantity typical of the impure ice age ices in Greenland) will enhance strain rate by no more than 30% and most likely will have an immeasurably small effect. A similar conclusion has been reached by *Lipenkov et al.* [1989] on the basis of analyses of Vostok ice and by *Paterson* [1991] on the basis of analyses of borehole tilt at Law Dome [*Etheridge*, 1989].

4.5. Role of Rock Particles

We find no evidence for a direct influence of rock particles on rheology, as even an extremely restrictive confidence interval (60 %) for β includes $\beta = 0$. However, optimized models all have positive η, most probably indicating that a significant fraction of ions is stored on the surfaces of rock particles, possibly in liquid films [*Dash et al.*, 1995; *Cuffey et al.*, 1999]. The inferred fraction of ions stored at particle surfaces is

$$1 - \frac{1}{1+\eta A_r} = \frac{\eta A_r}{1+\eta A_r}, \tag{13}$$

which has a mean value in the Meserve ices of 0.065 (and is 0 to 0.17 at 95% confidence). Suppose all this ion storage occurs in ice-rock interfacial liquid films of average thickness h. Then the fraction of stored ions is also $hA_rC_hC^{-1}$, where C_h and C are concentrations in

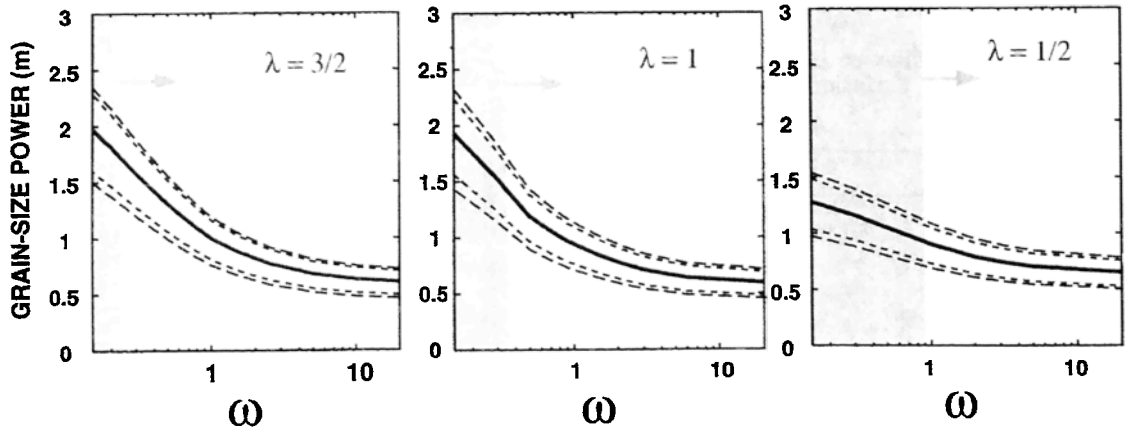

Figure 8. Inferred grain size power dependence m in D^{-m} as a function of grain importance parameter ω. Results are shown for three specific values of solute exponent λ. The 90 and 95% confidence intervals for m at given ω are shown. In addition, the 95% confidence region for ω lies to the right of the shaded areas.

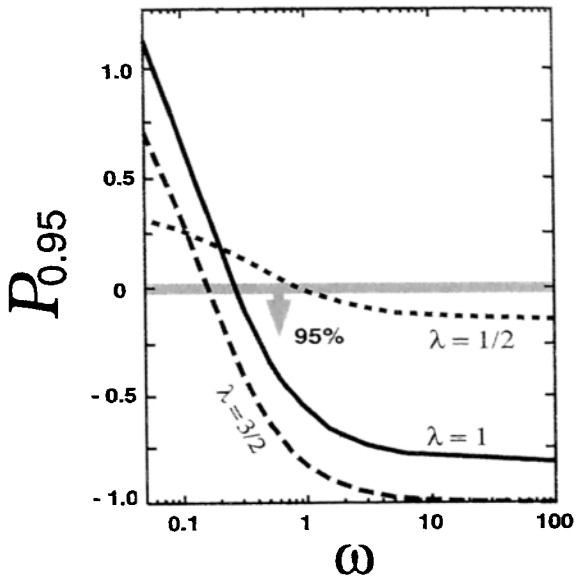

Figure 9. Model performance as a function of ω and λ. The $\lambda = 1/2$ models, though acceptable at 95% confidence, as indicated by the threshold, are not very good.

the film and the bulk, respectively. If C_h is determined by the NaCl liquidus and so is an ~3 mol L^{-1} brine (at -17°C [*Wettlaufer et al.*, 1997]), then using the measured average value of $C/A_r = 2.6 \times 10^{-5}$m mol L^{-1}, h is ~55 nm on average (or in the range 0 to 150 nm according to the 95% confidence interval on η). This h is consistent with the film thickness (20 to 40 nm) inferred by *Cuffey et al.* [1999] on the basis of analysis of measured slip at ice-rock interfaces at the study site.

5. Discussion

The grain size dependence likely results from an explicitly grain-size-dependent deformation mechanism such as grain boundary sliding or diffusional creep. *Goldsby and Kohlstedt* [1997] and *Duval et al.* [1983] suggest that for these mechanisms, strain rate is inversely proportional to grain size raised to a power m of 1.4, or 2 to 3, respectively, either of which is consistent with our results. The alternative interpretation, that grain size is determined by strain rate, which here is determined by an unidentified and unmeasured quantity, seems highly unlikely. This would imply that substantial variations of strain rate are caused by a physical quantity that is neither grain size nor a major impurity nor a consequence of mechanical anisotropy and which is not correlated with either impurities or fabrics.

Physically, the success of a model that multiplies rather than adds effects of grain size and chemistry suggests that ions are partly affecting viscosity through a grain-size-dependent deformation mechanism. As discussed above, concentrated impurities at grain boundaries will enhance liquid layers there, and such layers likely facilitate grain boundary sliding and mass transfer along grain boundaries. The latter will help polycrystalline ice accommodate [*De la Chapelle et al.*, 1999] the incompatible deformations that are a necessary consequence of the strong single-crystal mechanical anisotropy. Thus, as explained by *Barnes et al.* [1971], the ions are acting to increase the effective temperature of the polycrystal, with respect to the relative importance of different deformation mechanisms and accommodation processes.

Concerning the ionic term E_{*C}, the large variation of ion concentrations in the stratified ices of our study site makes it possible to constrain the nonlinearity λ to some extent. However, the generally small size of the ionic terms and the partial correlation with crystal size make the confidence limits on λ broad. At 90% confidence, λ is in the range 0.52 to 3.5. This precludes a very low sensitivity ($\lambda < 0.5$) and therefore argues against a saturation value of concentration beyond which further addition of impurity has no effect [*Nakamura and Jones*, 1970]. This is consistent with ions acting through grain boundary effects rather than through changes of lattice properties. The best fit λ, ~1.5, has very little variation as a function of the parameter ω.

An important result of sensitivity tests is that our inference of low sensitivity to ionic content is not qualitatively sensitive to our treatment of rock impurity. If we assume no role for rock particles at all (i.e., we assume that there is no ion storage or direct softening effect) by setting $\eta = \beta = 0$ in equation (2) and recalculating the optimal solution, inferred γ are reduced to 0.4 of their optimal solution values. This strengthens

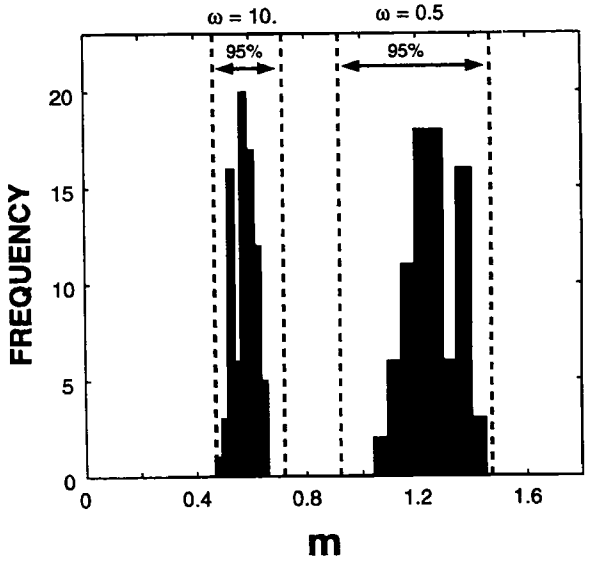

Figure 10. Frequency distribution of optimal m generated by Monte Carlo simulation for two fixed values of ω. The dashed lines show the 95% confidence interval derived from the assumption that the distribution is χ^2 as described in the text. The assumption is clearly valid.

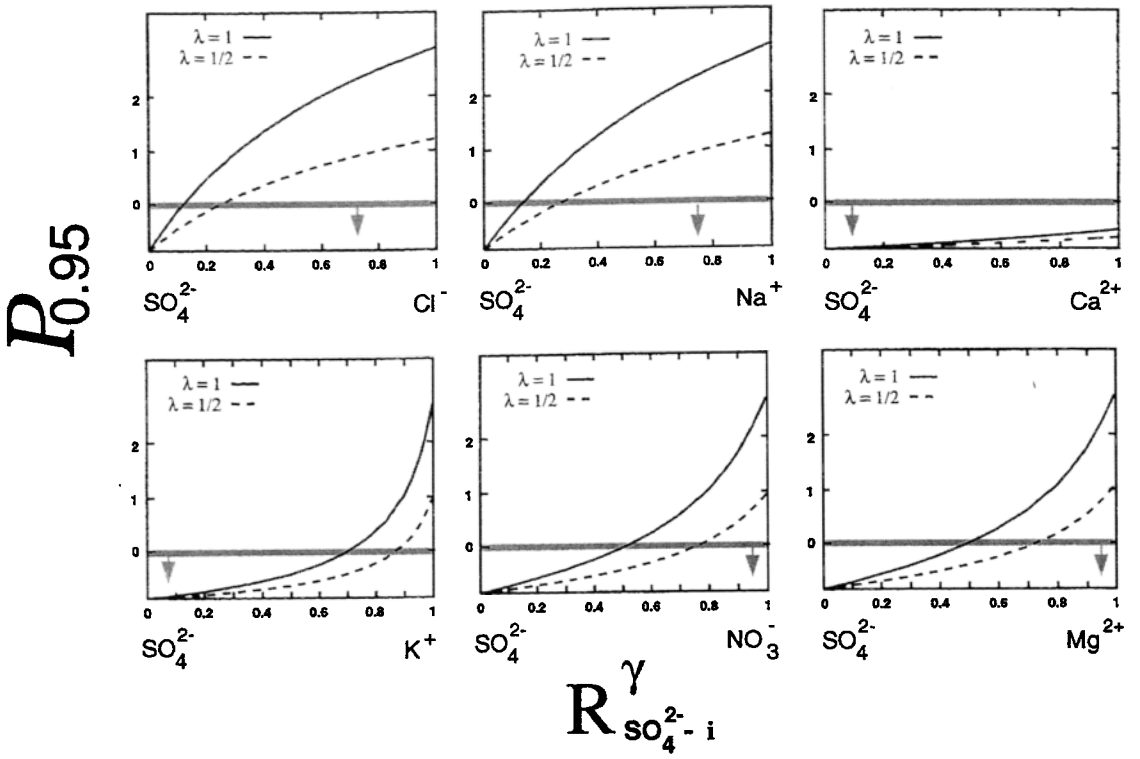

Figure 11. Model performance as a function of relative softening efficacy of six ions, relative to SO_4. The 95% confidence region is below the bars, as indicated by the arrows. When the x axis value is 0.5 in these graphs, the two ions considered have an equal per molar softening effect. At the 0 and 1 positions on the x axis, the indicated ion is much more effective than the other.

the conclusion that ionic sensitivities are low. Inferred γ are not dependent on the value for ω (Figure 13).

The optimal models all ascribe an important softening effect to C_+, which we presume to be acidity. This results primarily from the correlation of C_+ with the strain rate increase in the upper part of the D grid (Figure 2), which is only partially explained by variations of grain size and principal ions. The main results of this paper are insensitive to our use of a C_+ term. If we set $\gamma^+ = 0$ and recalculate the optimal solution, the optimal grain size power m decreases by 1.4%, and $\gamma_{1.5}^{SO_4}$ increases by 15%.

However, the sensitivity of strain rate enhancement to acidity is important in the context of flow of the Greenland ice sheet because Holocene ice is acidic whereas glacial-age ice is not. Unfortunately, this sensitivity is very poorly constrained in our analysis. We have explored a class of models in which the power law dependence for C_+ is different from that for the principal ions (such as sulphate). For example, we have treated the ion softening term as $\gamma_\lambda^{SO_4} C_{SO_4}^\lambda + \gamma_{\lambda^*}^+ C_+^{\lambda^*}$, where λ^* is an arbitrary positive constant. The resulting λ^* is very poorly constrained and at 95% confidence is in the range (0.02,3.5), with an optimal value of $\lambda^* = 0.4$. Examples of corresponding sensitivities are $\gamma_1^+ = 0.0231$ and $\gamma_{0.1}^+ = 0.501$ for λ=1 and λ=0.1, respectively.

Concerning anisotropic flow laws, our strain rate analysis has revealed nothing about the relative merits of the uniform stress versus uniform strain rate assumptions. The optimal model uses the uniform stress model ($e_{AS} = 0.2$). However, the 90% confidence interval on e_{AS} is (0,0.92), indicating no distinction can be made. This failure is not surprising, because the predictions of these models differ by only a constant multiple for a symmetrical single-maximum fabric normal to the shear plane. More complicated fabrics are needed for this type of analysis to have resolving power in this regard.

6. Conclusion

Analyses of in situ deformation beneath Meserve Glacier offer evidence that the deformation properties of polycrystalline glacier ice can depend directly on crystal size at stresses and temperatures typical of polar ice sheets and glaciers. This suggests an important role for grain boundary processes as suggested by *Barnes et al.* [1971] and supports *Goldsby and Kohlstedt*'s [1997] and *Peltier*'s [1998] view that Glen's law reflects contributions from both grain-size-dependent and -independent deformation mechanisms. However, our analyses do not constrain which size-dependent mechanism is operative and, in particular, do not argue for or against the grain boundary sliding mechanism of *Goldsby and Kohlstedt* [1997].

The most parsimonious expression of our results is that ice viscosity is proportional to $D^{-0.6}$ in our data.

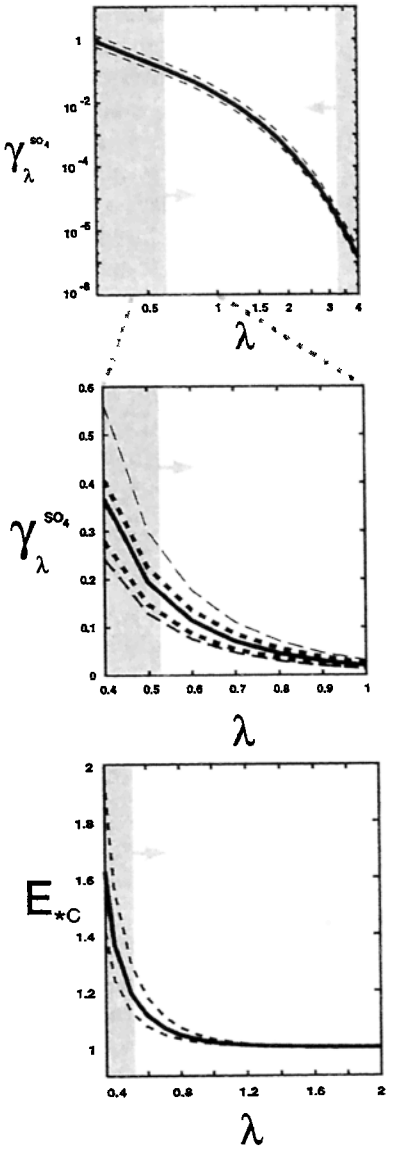

Figure 12. Inferred sensitivity of strain rate to the dominant impurity (here taken to be sulphate), and the corresponding strain rate enhancement for the interval λ = [0.4,2]. The shaded regions are unacceptable at 90% confidence. (top) Log-log scale and (middle and bottom) linear-linear scale.

We have fully explored a viscosity model that includes free parameters to describe effects of chemical impurities, solid impurities, crystal fabrics, and stress variations. No region of parameter space was found that contained an acceptable model without a direct dependence on D.

Further, we found that some ions (possibly SO_4 or Ca) are important softening agents at high concentrations but probably not at concentrations typical of the ice sheets (as recognized by *Budd and Jacka* [1989]). When ions do affect viscosity, they act, in part, to enhance grain-size-dependent mechanisms. This is consistent with the view that chemical impurities increase the effective temperature of ice polycrystals with respect to deformation mechanisms, as envisioned by *Barnes et al.* [1971] and subsequent investigators like *Fisher* [1987]. Rock particles are probably irrelevant at concentrations found in ice sheets. Thus we argue that viscosity enhancement of glacier ice is almost entirely controlled by its physical properties: texture and fabric.

We find no evidence that dirty basal layers have low viscosity because of a direct influence of rock content. Instead, we suggest that small crystals and strong fabrics are responsible for the low viscosities. Chemical impurities can contribute in very impure layers like those beneath Meserve.

All of these conclusions should be viewed as hypotheses; we are keenly aware of the need for more data. Further studies of in situ deformation, preferably supported by direct measurements of stress, will shed light on these rheologic issues and will continue to complement laboratory experiments. Future work may also help resolve the most important ambiguity in the Meserve Glacier data, which is the relative magnitude of grain-size-dependent versus grain-size-independent mechanisms at a given grain size (as given by our parameter $\tilde{\omega}$).

Appendix A: The c Axis Fabrics and Stress

A1. Measurement of c Axis Fabrics

For 35 of the thin sections we measured c axis orientations for at least 100 grains (Figures A1 and A2), using crossed polarizers and a Rigsby stage [*Langway*, 1958]. Proper corrections for refraction effects were made, following *Kamb* [1962]. Selection of grains for orientation measurement was randomized by dropping a pointer onto the thin section. Thus our c axis fabrics

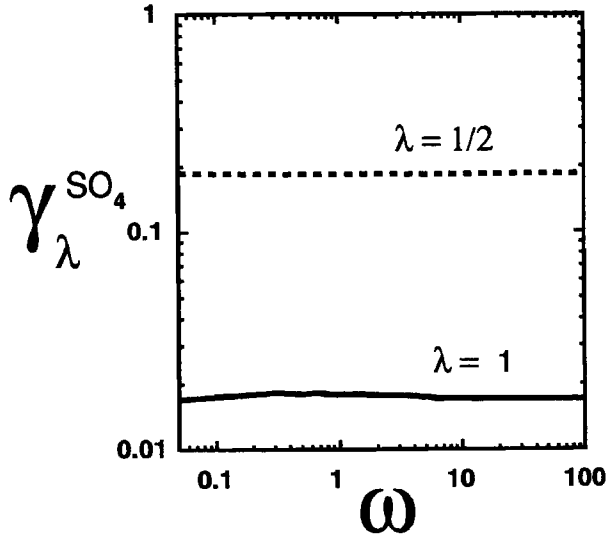

Figure 13. The inferred sensitivity to the dominant impurity (here taken to be sulphate) as a function of ω for two values of λ.

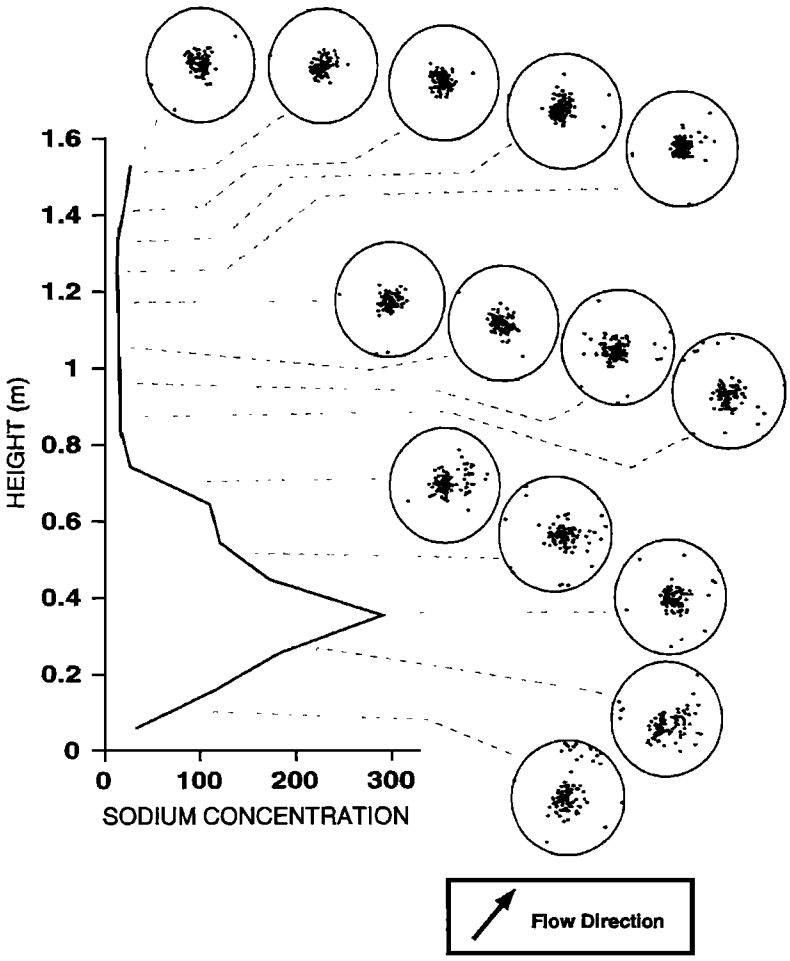

Figure A1. The c axis orientations for thin sections near the U grid and corresponding stratigraphic positions (stratigraphy here represented by the micromolar sodium concentration). Each thin section has at least 100 measured orientations. Note the generally stronger clustering of c-axes high in the profile.

are area-weighted, which is proper for rheologic calculations. Thin sections were taken parallel to the plane of shear, with a ±10°uncertainty in the orientation of the normal to the thin section and a ±10°uncertainty in the azimuth relative to the flow direction. In many cases, the uncertainty on the orientation relative to the shear plane was smaller because visible, bed-parallel strata guided the cutting of the thin section. The azimuth is known so well because the elongate bubbles provide a built-in directional indicator [*Holdsworth*, 1974].

The amber ices again presented a special difficulty owing to their very small grain sizes (0.6 mm apparent diameter seen in section). In his study of Meserve ice petrography, *Anderton* [1974] did not obtain any fabric data for the amber ices but noted that they appeared to have a strong fabric. We were able to obtain fabric data by using optical binocular magnifying glasses (manufactured by Donegan Optical Company, Lenexa, Kansas) which provided an effective magnification of ~2×. The main difficulty proved not to be the uncertainty in identifying the angular position of maximum extinction (as one might suppose) but rather the task of tracking a single grain through rotations of the stage. A successful measurement was obtained in only ~30% of the attempts. This, plus the small absolute sizes, almost certainly introduced a "large-grain" bias to the resulting fabric data in addition to the intentional one for proper area weighting.

Excepting this problem, we are confident that the fabric data we obtained for amber ices are accurate. The amber ice fabrics are quite similar to the fabrics obtained from white ices, with the strong shear-normal single maximum that is characteristic of simple shear flows. For one of the amber ice thin sections we prepared a companion section from amber ice a few centimeters higher in the column but with a tilt of 35°relative to the original. The inferred fabric had 7°broader dispersion of c-axes, most likely reflecting a greater error in identifying extinction position for grains that are significantly tilted relative to the thin section plane or its normal.

A2. Using Fabric Data

We calculate $\dot{\epsilon}^F$ directly from c axis fabric data and assumed stress tensors according to *Azuma* [1994] and

van der Veen and Whillans [1994], the latter being an application of the model due to Sachs [see *Castelnau et al.*, 1996]. We denote calculations of $\dot{\epsilon}^{F}$ using the Azuma and Sachs models as $\dot{\epsilon}^{F,A}$ and $\dot{\epsilon}^{F,S}$, respecitvely.

Considering a single crystal, assumed to deform by basal glide in systems k with Burger's vectors B_i^k in the global coordinate system x_i (i.e., a convenient coordinate system for the glacier as a whole), the resolved shear stress on the basal planes of a crystal with c axis orientation vector c_j is $\tau^k = B_i^k c_j \tau_{ij}$. The tensor $B_i^k c_j$ is called the Schmid tensor and denoted S_{ij}^k.

In the Sachs formulation the stress acting on each crystal is assumed to be simply the bulk stress τ_{ij} and the bulk deformation is the average over all crystals (N in number) of the deformations caused by the shear stress resolved on the basal planes:

$$\dot{\epsilon}_{ij}^{F,S} = \frac{A_S}{N} \sum_{g=1}^{N} \sum_{k} S_{ij}^{k,g} \left(S_{pq}^{k,g} \tau_{pq} \right)^n , \qquad \text{(A1)}$$

where the sums over spatial directions $p, q = 1, 2, 3$ are indicated by repeated indices and the superscript F, S indicates the Sachs model is being used. A superscript F, A will indicate the Azuma model.

The Azuma formulation assumes the slip direction is the direction of maximum resolved stress on the basal planes [*Azuma*, 1994, Appendix 1]), with a corresponding Schmid tensor S_{ij}^*. The average value of S_{ij}^* for all grains is computed (effectively replacing the polycrystal with a single crystal having average properties), and the uniform bulk deformation rate is

$$\dot{\epsilon}_{ij}^{F,A} = A_A \langle S_{ij}^* \rangle \left(\langle S_{pq}^* \rangle \tau_{pq} \right)^n , \qquad \text{(A2)}$$

where the angle brackets indicate the average over all N grains and again there are sums over $p, q = 1, 2, 3$. The prefactors differ by $A_A = 2A_S$ [*Thorsteinsson et al.*, 1999].

To use these formulae for calculating $\dot{\epsilon}_{ij}^{F}$, we need to specify how the stress varies relative to its mean and the relative magnitudes of the various deviatoric stress components (the mean value is unimportant because we treat the prefactor A as a free parameter). We adopt

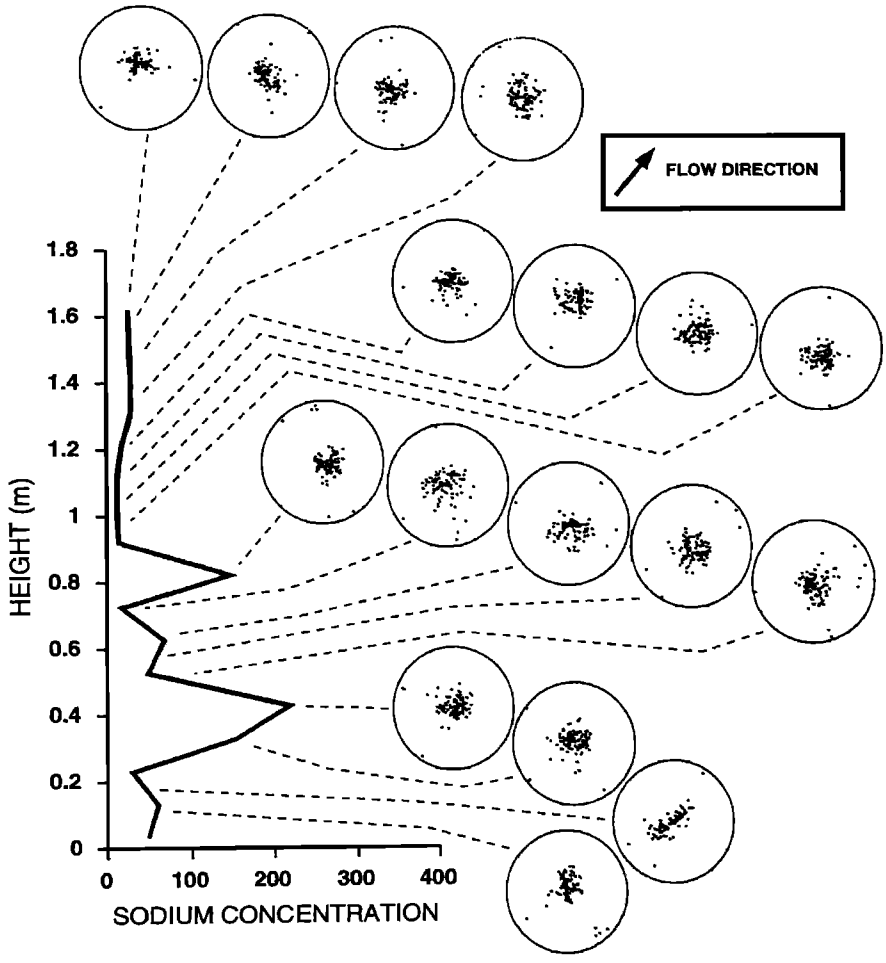

Figure A2. The c axis orientations for thin sections near the D grid and corresponding stratigraphic positions (stratigraphy here represented by the micromolar sodium concentration). Each thin section has at least 100 measured orientations. Not shown here are five additional sections which show the same lack of variability.

two end-member views of the stress, one in which the stress perturbation caused by the tunnel is ignored, and one in which we maximize its effect. This stress perturbation causes tunnel closure, and we have measured tunnel closure rates at one cross section in the tunnel, 15 m from the tunnel entrance. The closure rate was determined by measuring relative distance changes between markers (metal bolts inserted and frozen into drill holes in the tunnel wall) arranged in a line spanning both walls and ceiling of the tunnel (following *Holdsworth* [1974]). Thus we have directly measured the closure velocity into the tunnel, and the shear strain rate caused by this motion relative to the no-slip bed (the small slip rate reported in *Cuffey et al.* [1999] did have a component into the tunnel, but this few mm yr^{-1} slip is unimportant in this context).

Define a coordinate system with (x_1, x_2, x_3) being flow-parallel, flow-normal bed-parallel, and bed-normal directions, respectively (these three also being subparallel to the long axis of the tunnel, into the tunnel normal to the tunnel side walls, and bed-normal). The stresses associated with the closure motions are a longitudinal closure stress τ_{22} acting normal to the tunnel wall and a closure shear stress τ_{23} acting on horizontal planes but perpendicular to the dominant downflow shear stress τ_{13}.

We assume the dominant shear stress acting on the ice τ_{13} depends on height above the bed (x_3) and is enhanced by increases in void ratio V_b and has the form

$$\tau_{13} = \frac{\left(1 - \frac{x_3}{H}\right)^{\nu}}{(1 - V_b)}, \tag{A3}$$

in which x_3 is zero at the bed, H is the ice thickness, V_b is the volume fraction of bubbles, and ν is the power characterizing the effective spatial variation of stress with depth. This ν does not necessarily equal unity as it would if the weight of overburden controls the stress because it also reflects the variation in shear stress due to gradients in longitudinal stress τ_{11} which we do not know but which will generally oppose the upward decrease of τ_{13} caused by the decrease of overburden. Most importantly, the magnitude of τ_{13} variation is almost certainly small due to the small size of our strain grids relative to the glacier thickness. We have used values for ν of 0.0, 0.3, 0.7, and 1.0 and found that none of the results presented in this paper depend on this number in any significant fashion. Our strain rate measurements provide a direct measurement of longitudinal strain rate along-flow, which is approximately zero. This may primarily reflect the near-vertical c axis fabric and therefore does not mean the longitudinal stress τ_{11} has a negligible effect on the (unknown) τ_{13} gradient.

With regard to the tunnel effects, the two end-member stresses we consider are case 1 (the tunnel has no effect on the stress):

$$\tau_{22} = 0 \tag{A4}$$

$$\tau_{23} = 0 \tag{A5}$$

and case 2 (there is a longitudinal stress into the tunnel, with a magnitude proportional to closure velocity and there is a shear stress associated with tunnel closure over a no-slip bed):

$$\tau_{22} = \tau_{22}^{\max} \left[\frac{u_c}{u_c^{\max}}\right]^{1/n} \tag{A6}$$

$$\tau_{23} = \tau_{13} \left[\frac{\dot{\epsilon}_{23}}{\dot{\epsilon}_{13}}\right]^{1/n}. \tag{A7}$$

For the maximum value $\tau_{22}^{\max}$ of the closure stress we use one-quarter of the overburden pressure, or 1/4 (2 bars) = 0.5 bar, which we estimate to be approximately equal to τ_{13}. One may be inclined to use one-half the overburden pressure for the maximum deviatoric stress $\tau_{22}^{\max}$, but for a nonlinear fluid such as ice the large stress-coupling lengths cause a broad low-pressure zone around a subglacial tunnel [*Weertman*, 1972]. In any case, these calculations are illustrative. The u_c in A6 is measured closure rate, which has a maximum value of $u_c^{\max}$= 0.04 m yr^{-1}, and the ratio of the two bed-parallel shears is estimated from the direct measurements. These two stress scenarios are used explicitly in (A1) and (A2) to calculate possible variations of the strain rate $\dot{\epsilon}_{13}$, which is the subject of all the analyses presented in this paper. The absolute value of the stress τ_{13} does not matter in this context, only the relative values.

According to these rheologic relations the shear $\dot{\epsilon}_{13}$ will depend only weakly on the other stress components due to the strong crystal fabrics (a result very different from the classic isotropic Glen's law if these stresses are used; however, if one assumed Glen's law to be true, the stresses estimated directly from closure measurements would be very small relative to the dominant shear, so the net result would be the same). We do not consider explicitly any stresses τ_{12}, as these will act as an intermediate case between these two extremes.

Thus we have four end-member stress-fabric models: Azuma with no tunnel stresses, Azuma with full tunnel stresses, Sachs with no tunnel stresses and Sachs with full tunnel stresses. Denote the $\dot{\epsilon}_{13}$ components of these $\dot{\epsilon}^{\mathrm{F,A}}$, $\dot{\epsilon}_{\mathrm{T}}^{\mathrm{F,A}}$, $\dot{\epsilon}^{\mathrm{F,S}}$, and $\dot{\epsilon}_{\mathrm{T}}^{\mathrm{F,S}}$, respectively. We describe the "true" $\dot{\epsilon}_{13}^{\mathrm{F}}$ as a linear mixture of these. Introduce two free model parameters e_{AS} and e_{T} which are each restricted to the range [0,1]. Then

$$\begin{aligned}\dot{\epsilon}_{13}^{\mathrm{F}} = {} & e_{\mathrm{AS}}\left[(1 - e_{\mathrm{T}})\dot{\epsilon}^{\mathrm{F,A}} + e_{\mathrm{T}}\dot{\epsilon}_{\mathrm{T}}^{\mathrm{F,A}}\right] \\ & + (1 - e_{\mathrm{AS}})\left[(1 - e_{\mathrm{T}})\dot{\epsilon}^{\mathrm{F,S}} + e_{\mathrm{T}}\dot{\epsilon}_{\mathrm{T}}^{\mathrm{F,S}}\right].\end{aligned} \tag{A8}$$

Appendix B: Common Reference Frame

We determined average chemical and physical properties for each of the thirty-three 0.1 m intervals using linear combinations (which are weighted averages) of the measured values from samples in the stratigraphic lay-

ers composing the intervals. More precisely, the value for the jth property in the ith grid interval, P_{ji}, is calculated in terms of the k measured values for this property M_{jk} as

$$P_{ji} = \sum_k a_{ik} M_{jk}, \tag{B1}$$

where the coefficients a_{ik} are restricted to the range [0,1] and subject to the requirement $\sum_k a_{ik} = 1$ (typically there are one to four nonzero terms in the sum). The a_{ik} values were selected a priori from stratigraphic maps of the tunnel walls that show explicitly (1) that specific stratigraphic layers contained in the strain rate grid intervals correlate precisely with certain stratigraphic layers in the measured profiles of ice properties and (2) that the 0.1 m (vertical) by 0.5 m (horizontal) areas of ice surface centered on each of the 33 strain grid rows consist of quantifiable proportions of the various stratigraphic layers.

The extrapolation/interpolation procedure (1) is justified because the between-layer variability of ice properties is much greater than the along-flow variability, a direct consequence of large shear strain. For example, the topmost amber ice layer in the D grid was sampled both 2 m upflow and 1 m downflow from the grid (Table 4), and the micromolar ionic concentration differs by 10% between these two sites. For the white ice 0.2 m above the top of this amber, the upflow and downflow difference is 17%. By contrast, the amber and white ices differ in average ion content by a factor of 920% at the upstream site and 990% at the downstream.

The partitioning procedure (2) is more difficult to justify conceptually, as it contains two approximations: that the rheologic properties of a mixed layer equal a linear mixture of the rheologic properties of sublayers, and that the relative proportions of various layers seen on the strain grid wall equal the volumetric proportions to whatever depth into the wall is relevant to determining the strain rate. However, the complete range of variability between stratigraphic layers is unambiguously represented because many of the grid levels require no partitioning at all, being all one layer. Moreover, the stratigraphic layers are generally characterized by a horizontal span much greater than the size of the strain grids and much greater than their vertical extent (i.e., the stratigraphic units are either continuous layers or very elongate lensoids).

Table 4. Comparison of Major Ion Concentrations for Two Stratigraphic Horizons Between Two Locations Separated by 2.5 m Along Flow[a]

Site	Ice Type	Na^+	Ca^{2+}	Cl^-	SO_4^{2-}
Upflow	Amber	161	50	190	41
Downflow	Amber	190	52	198	35
Upflow	White	14	6	23	5
Downflow	White	12	7	22	9

[a]Units are μmol L^{-1}.

Notation

A	flow law prefactor.
A_A	flow law prefactor for the Azuma formulation.
A_r	surface area of ice-rock interface per volume of ice.
A_S	flow law prefactor for the Sachs formulation.
a_{ik}	fractional contribution of the kth ice sample to the ith vertical interval on a strain grid.
C_i	bulk concentration of chemical impurity i.
C_+	bulk concentration of unbalanced positive charges.
D	crystal diameter, equal to 1.5 times average intercept length.
E	strain rate enhancement.
E_*	strain rate enhancement not due to fabric.
E_{*C}	strain rate enhancement due to chemical impurities.
E_{*D}	strain rate enhancement due to grain size.
e_{AS}	trade-off parameter for Azuma versus Sachs anisotropic flow relations.
e_T	trade-off parameter for two views of tunnel stress effects.
H	glacier thickness.
i, j, k	dummy indices.
M_{jk}	measured value of j for the kth ice sample.
m	exponent pertaining to dependence of E_* on D.
n	stress exponent of flow laws.
P_{ji}	value of any measured quantity j in the ith vertical section of a strain grid.
$\mathcal{P}_{0.95}$	index of fit relative to (as a multiple of) 95% confidence.
$\mathcal{P}_{0.995}$	index of fit relative to (as a multiple of) 99.5% confidence
R^{γ}_{a-b}	relative per-molar sensitivity of chemical species a to species b.
S_{ij}	Schmid tensor (standard definition).
S^*_{ij}	Schmid tensor (Azuma definition).
T	temperature.
V_b	volume of void (bubble) per volume of ice.
V_r	volume of rock per volume of ice.
x_1	spatial coordinate parallel to flow.
x_2	horizontal spatial coordinate normal to flow.
x_3	spatial coordinate normal to bed.
β	linear sensitivity of strain rate to V_r.
γ^i_λ	per molar sensitivity of E_{*C} to C^λ_i.
$\Delta\chi^2$	increase of χ^2 for a model relative to that for the optimal model, equal to $\chi^2 - \chi^2_{min}$.
$\dot{\epsilon}$	strain rate tensor.
$\dot{\epsilon}^F$	strain rate tensor dependent on c axis fabric for pure ice and constant grain size.
$\dot{\epsilon}^m_i$	model strain rate value for ith interval of the strain grids.
$\dot{\epsilon}^o_i$	observed strain rate value for ith interval of the

strain grids.

$\dot{\epsilon}^{F,A}$ fabric-only anisotropic strain rate law as given by Azuma, and calculated without tunnel stresses.

$\dot{\epsilon}^{F,S}$ fabric-only anisotropic strain rate law as given by Sachs and calculated without tunnel stresses.

$\dot{\epsilon}_T^{F,A}$ fabric-only anisotropic strain rate law as given by Azuma and calculated with tunnel stresses.

$\dot{\epsilon}_T^{F,S}$ fabric-only anisotropic strain rate law as given by Sachs and calculated with tunnel stresses.

η parameter which multiplies A_r to determine magnitude of ion storage on rock particle surfaces.

λ exponent on ionic concentration in E_{*C}.

σ_ϵ standard deviation of strain rate measurements.

σ_P standard deviation of modelled strain rate measurements generated by random errors in all input measured quantities.

τ deviatoric stress tensor.

χ^2 summed mismatch of modeled and measured strain rates.

χ^2_{min} χ^2 value for the optimal model.

ω grain importance parameter, equal to $\tilde{\omega}/(1-\tilde{\omega})$.

$\tilde{\omega}$ grain importance parameter which defines the relative magnitude of grain-size-dependent and -independent deformation, at a grain size of 1 mm (3).

ω_a ω for a model in which chemistry and size-dependent terms are strictly additive.

Acknowledgments. We thank G. Holdsworth and P. Lombard for encouragement and suggestions. We also thank J. Wright of Silverton, Colorado, for guidance on tunnel engineering; Al Rasmussen for reducing the strain rate data; and M. Twickler, P. Mayewski, and S. Lea for facilitating the chemical and particle analyses. We further thank Y. Moh and J. Szolnicki for assistance. Part of this work was performed at the Department of Energy's Pacific Northwest National Laboratory (W.R. Wiley Environmental Molecular Sciences Laboratory), a national scientific user facility, in collaboration with Scott Lea. Research funded by NSF OPP-941838-1 to H.C. and B.H., and UC Berkeley funds to K.C.

References

Alley, R.B., Fabrics in polar ice sheets: Development and prediction, *Science, 240*, 493-495, 1988.

Alley, R.B., Flow-law hypotheses for ice sheet modelling, *J. Glaciol., 38*, 245-256, 1992.

Alley, R.B., J.H. Perepezko, and C.R. Bentley, Grain growth in polar ice, II, Application, *J. Glaciol., 32*, 425-433, 1986.

Anderton, P.W., Ice fabrics and petrography, Meserve Glacier, Antarctica, *J. Glaciol., 13*, 285-306, 1974.

Ashby, M.F., On the Orowan stress, in *Physics of Strength and Plasticity*, edited by A.S. Argon, pp. 113-131, MIT Press, Cambridge, Mass., 1969.

Ashby, M.F., The influence of particles on boundary mobility, in *Recrystallization and Grain Growth of Multiphase and Particle Containing Materials*, edited by N. Hansen, A.R. Jones, and T. Leffers, pp. 325-336, Riso Nat. Lab., Roskilde, Denmark, 1980.

Azuma, N., A flow law for anisotropic ice and its application to ice sheets, *Earth Planet. Sci. Lett., 128*, 601-614, 1994.

Azuma, N., and K. Goto-Azuma, An anisotropic flow law for ice-sheet ice and its implications, *Ann. Glaciol., 23*, 202-208, 1996.

Azuma, N., and A. Higashi, Formation processes of ice fabric pattern in ice sheets, *Ann. Glaciol., 6*, 130-134, 1985.

Barnes, P., D. Tabor and J.C.F. Walker, The friction and creep of polycrystalline ice, *Proc. R. Soc. London, Ser. A, 324*, 127-155, 1971.

Buck, C.F., P.A. Mayewski, M.J. Spencer, S. Whitlow, M.S. Twickler, and D. Barrett, Determination of major ions in snow and ice cores by ion chromatography, *J. Chromatogr., 594*, 225-228, 1992.

Budd, W.F., and T.H. Jacka, A review of ice rheology for ice sheet modelling, *Cold Reg. Sci. Technol., 16*, 107-144, 1989.

Castelnau, O., P. Duval, R. A. Lebensohn, and G.R. Canova, Viscoplastic modeling of texture development in polycrystalline ice with a self-consistent approach: Comparison with bound estimates, *J. Geophys Res. 101*, 13,851-13,868, 1996.

Cuffey, K.M., H. Conway, B. Hallet, A.M. Gades and C.F. Raymond, Interfacial water in polar glaciers and glacier sliding at -17°C, *Geophys. Res. Lett., 26*, 751-754, 1999.

Cuffey, K.M., H. Conway, A.M. Gades, B. Hallet, R. Lorrain, J.P. Severinghaus, E.J. Steig, B. Vaughn, and J.W.C. White, Entrainment at cold glacier beds, *Geology, 28*, 351-354, 2000.

Cuffey, K.M., T. Thorsteinsson, and E.D. Waddington, A renewed argument for crystal size control of ice sheet strain rates, *J. Geophys. Res.*, this issue.

Dahl-Jensen, D., and N.S. Gundestrup, Constitutive properties of ice at Dye 3, Greenland, *IAHS Publ., 170*, 31-43, 1987.

Dahl-Jensen, D.J., T. Thorsteinsson, R.B. Alley, and H. Shoji, Flow properties of the ice from the Greenland Ice Core Project ice core: The reason for folds?, *J. Geophys. Res. 102*, 26,831-26,840, 1997.

Dash, J.G., H. Fu, and J. Wettlaufer, The premelting of ice and its environmental consequences, *Rep. Prog. Phys., 58*, 115-167, 1995.

De La Chapelle, S., H. Milsch, O. Castelnau, and P. Duval, Compressive creep of ice containing a liquid intergranular phase: rate-controlling processes in the dislocation creep regime, *Geophys. Res. Lett., 26*, 251-254, 1999.

Durham, W.B., S.H. Kirby, and L.A. Stern, Effects of dispersed particulates on the rheology of water ice at planetary conditions, *J. Geophys. Res. 97*, 20,883-20,897, 1992.

Duval, P., and H. LeGac, Does the permanent creep rate of polycrystalline ice increase with crystal size?, *J. Glaciol., 25*, 151-157, 1980.

Duval, P., M.F. Ashby, and I. Anderman, Rate-controlling processes in the creep of polycrystalline ice, *J. Phys. Chem., 87*, 4066-4074, 1983.

Echelmeyer, K., and W. Zhongxiang, Direct observations of basal sliding and deformation of basal drift at sub-freezing temperatures, *J. Glaciol., 33*, 83-98, 1987.

Echelmeyer, K. A., W.D. Harrison, C. Larsen, and J.E. Mitchell, The role of the margins in the dynamics of an active ice stream, *J. Glaciol., 40*, 527-538, 1994.

Etheridge, D.M., Dynamics of the Law Dome ice cap, Antarctica, as found from bore-hole measurements, *Ann. Glaciol., 12*, 46-50, 1989.

Fisher, D.A., Enhanced flow of Wisconsin ice related to solid conductivity through strain history and recrystallization, *IAHS Publ., 170*, 45-51, 1987.

Fisher, D.A., and R.M. Koerner, On the special rheological properties of ancient microparticle-laden Northern Hemisphere ice as derived from bore-hole and core measure-

ments, *J. Glaciol., 32*, 501-510, 1986.
Glen, J.W., The creep of polycrystalline ice, *Proc. R. Soc. London, Ser. A, 228*, 519-538, 1955.
Goldsby, D.L., and D.L. Kohlstedt, Grain boundary sliding in fine-grained Ice I, *Scr. Mater., 37*, 1399-1406, 1997.
Gow, A.J., D.A. Meese, R.B. Alley, J.J. Fitzpatrick, S. Anandakrishnan, G.A. Woods and B.C. Elder, Physical and structural properties of the Greenland Ice Sheet Project 2 ice core: A review, *J. Geophys. Res. 102*, 26,559-26,576, 1997.
Holdsworth, G., Meserve Glacier, Wright Valley Antarctica, part 1, Basal processes, *Rep. 37*, Inst. Polar Stud., Columbus, Ohio, 1974.
Holdsworth, G., and C. Bull, The flow law of cold ice: Investigations on Meserve Glacier, Antarctica, *IAHS Publ., 86*, 204-216, 1970.
Hooke, R.L., B.H. Dahlin and M.T. Kauper, Creep of ice containing dispersed fine sand, *J. Glaciol., 11*, 327-36, 1972.
Jacka, T.H., Laboratory studies on relationships between ice crystal size and flow rate, *Cold Reg. Sci. Technol., 10*, 31-42, 1984.
Jones, S.J., and H.A.M. Chew, Effect of sample and grain size on the compressive strength of ice, *Ann. Glaciol., 4*, 129-132, 1983.
Jun, L., T.H. Jacka, and W.F. Budd, Deformation rates in combined compression and shear for ice which is initially isotropic and after the development of strong anisotropy, *Ann. Glaciol., 23*, 247-252, 1996.
Kamb, W.B., Refraction corrections for universal stage measurements, I, Uniaxial crystals, *Am. Mineral., 47*, 227-245, 1962.
Koerner, R.M., and D.A. Fisher, Discontinuous flow, ice texture, and dirt content in the basal layers of the Devon Island ice cap, *J. Glaciol., 23*, 209-222, 1979.
Langway, C.C., Ice fabrics and the universal stage, *SIPRE Tech. Rep. 62*, Snow, Ice, and Permafrost Res. Estab., Hanover, N.H., 1958.
Lipenkov, V.Y., N.I. Barkov, P. Duval, and P. Pimienta, Crystalline texture of the 2083 m ice core at Vostok Station, Antarctica, *J. Glaciol., 35*, 392-398, 1989.
Lliboutry, L., and P. Duval, Various isotropic and anisotropic ices found in glaciers and polar ice caps and their corresponding rheologies, *Ann. Geophys., 3*, 207-224, 1985.
Mayewski, P.A., L.D. Meeker, M.S. Twickler, S. Whitlow, Q. Yang, W.B. Lyons, and M. Prentice, Major features and forcing of high-latitude northern hemisphere atmospheric circulation using a 110,000-year-long glaciochemical series, *J. Geophys. Res. 102*, 26,345-26,366, 1997.
Menke, W., *Geophysical Data Analysis: Discrete Inverse Theory*, Academic, San Diego, Calif., 1989.
Nakamura, T., and S.J. Jones, Softening effect of dissolved hydrogen chloride in ice crystals, *Scr. Metall., 4*, 123-126, 1970.
Nye, J.F., The distribution of stress and velocity in glaciers and ice sheets, *Proc. R. Soc. London, Ser. A, 239*, 113-333, 1957.
Paren, J.G., and J.C.F. Walker, Influence of limited solubility on the electrical and mechanical properties of ice, *Nature Phys. Sci., 230*, 77-79, 1971.
Paterson, W.S.B., Why ice age ice is sometimes "soft", *Cold Reg. Sci. Technol., 20*, 75-98, 1991.
Paterson, W.S.B., *The Physics of Glaciers*, 3rd ed., 480 pp., Pergamon, Tarrytown, N.Y., 1994.
Peltier, W.R., Post glacial variations in the level of the sea: Implications for climate dynamics and solid-earth geophysics, *Rev. Geophys., 36*, 603-689, 1998.
Pimienta, P., P. Duval, and V. Y. Lipenkov, Mechanical behavior of ice along the 2040 m Vostok core, Antarctica, *Ann. Glaciol., 10*, 137-140, 1988.
Press, W.H., S.A. Teukolsky, W.T. Vetterling, and B.P. Flannery, *Numerical Recipes in FORTRAN: The Art of Scientific Computing*, 2nd ed., 963 pp., Cambridge Univ. Press, New York, 1992.
Riley, N.W., G. Noll, and J.W. Glen, The creep of NaCl-doped ice monocrystals, *J. Glaciol., 21*, 501-507, 1978.
Shoji, H., and C.C. Langway Jr., Flow-law parameters of the Dye 3, Greenland, deep ice core, *Ann. Glaciol., 10*, 146-150, 1988.
Thorsteinsson, T., E. D. Waddington, K. C. Taylor, R. B. Alley, and D. D. Blankenship, Strain rate enhancement at Dye 3, Greenland, *J. Glaciol., 45*, 338-345, 1999.
Underwood, E.E., *Quantitative Stereology*, Addison-Wesley-Longman, Reading, Mass., 1970.
van der Veen, C.J., and I.M. Whillans, Development of fabric in ice, *Cold Reg. Sci. Technol., 22*, 171-195, 1994.
Weertman, J., General theory of water flow at the base of a glacier or ice sheet, *Rev. Geophys., 10*, 287-333, 1972.
Wettlaufer, J.S., M.G. Worster, and H.E. Huppert, Natural convection during solidification of an alloy from above with application to the evolution of sea ice, *J. Fluid Mech., 344*, 291-316, 1997.

H. Conway, A. Gades, and C. Raymond, Geophysics Program, Box 351650, University of Washington, Seattle, WA 98195.

K. M. Cuffey, Department of Geography, 507 McCone Hall, University of California, Berkeley, CA 94720-4740. (kcuffey@socrates.berkeley.edu)

B. Hallet, Quaternary Research Center, University of Washington, Seattle, WA 98195.

S. Whitlow, Climate Change Research Center, Institute for the Study of Earth, Oceans and Space, University of New Hampshire, Durham, NH 03824.

(Received December 29, 1999; revised June 23, 2000; accepted June 30, 2000.)